CROSS-BRIDGE MODEL OF MUSCLE CONTRACTION

QUANTITATIVE ANALYSIS

EVAN EISENBERG, TERRELL L. HILL, AND YI-DER CHEN, *Laboratory of Cell Biology, National Heart, Lung, and Blood Institute and Laboratory of Molecular Biology, National Institute of Arthritis, Metabolism, and Digestive Diseases, National Institutes of Health, Bethesda, Maryland 20205 U.S.A.*

ABSTRACT We recently presented, in a qualitative manner, a cross-bridge model of muscle contraction which was based on a biochemical kinetic cycle for the actomyosin ATPase activity. This cross-bridge model consisted of two cross-bridge states detached from actin and two cross-bridge states attached to actin. In the present paper, we attempt to fit this model quantitatively to both biochemical and physiological data. We find that the resulting complete cross-bridge model is able to account reasonably well for both the isometric transient data observed when a muscle is subjected to a sudden change in length and for the relationship between the velocity of muscle contraction in vivo and the actomyosin ATPase activity in vitro. This model also illustrates the interrelationship between biochemical and physiological data necessary for the development of a complete cross-bridge model of muscle contraction.

1. INTRODUCTION

Recently, we published a cross-bridge model of muscle contraction based on current structural, biochemical, and physiological studies of cross-bridge action (1). This four-state, single-site model of cross-bridge action, which consists of two cross-bridge states detached from actin and two cross-bridge states attached to actin, was presented in a qualitative manner consistent with the theoretical formalism of Hill (2, 3). However, no attempt was made to fit current physiological and biochemical data quantitatively. The formalism is particularly well-suited to quantitative relation of equilibrium constants and rate constants obtained in biochemical studies to force, velocity, and elasticity measurements determined in physiological studies. Therefore in the present paper we examine the assumptions required for our model to quantitatively fit current biochemical and physiological data.

Perhaps the most important result of this modeling effort is that, making relatively few assumptions, we find that we can account reasonably well for both the force transient observed when a muscle fiber is subjected to a sudden change in length (4) and for the well-known relationship between the velocity of muscle contraction measured in vivo and the actomyosin ATPase activity measured in vitro (5).

2. BASIS OF THE CROSS-BRIDGE MODEL

The biochemical kinetic cycle on which our cross-bridge model is based is shown in Fig. 1 (6). The dashed lines in Fig. 1 *a* represent transitions that are assumed not to occur, whereas the heavy solid lines represent the dominant pathway (left to right) in the actomyosin ATPase

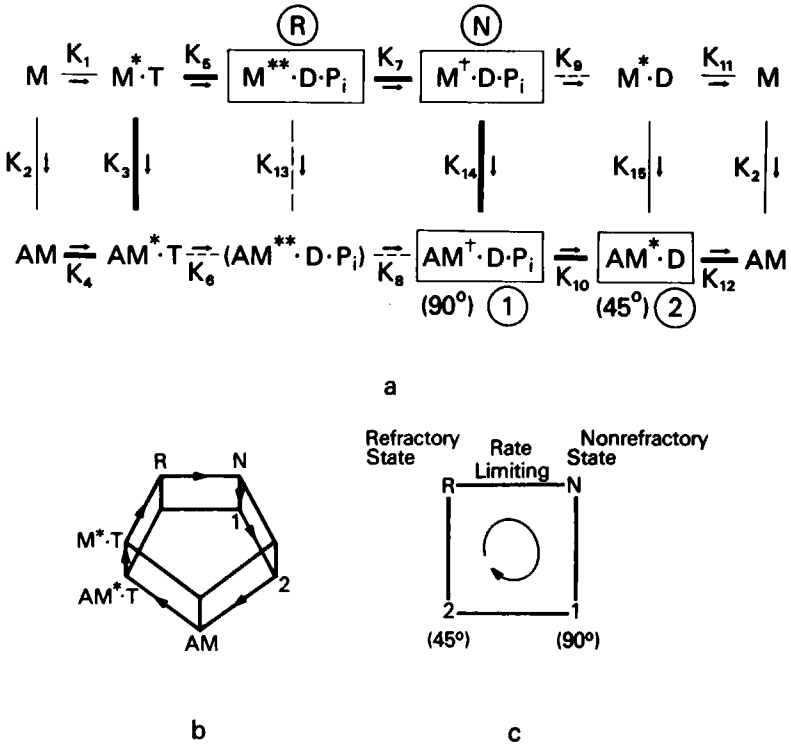

FIGURE 1 Biochemical scheme on which the cross-bridge model is based. (*a*) Complete biochemical scheme. Steps marked with dashed lines are assumed not to occur or to occur at a negligibly slow rate. Steps marked with a heavy solid line represent the dominant pathway of the actomyosin ATPase activity. The arrows show the direction in which the equilibrium constants are defined. Only the four boxed states are assumed to occur in significant concentrations in vivo. *R*, *N*, 1, and 2 are alternative names for these states (see text). (*b*) An alternative way of showing the biochemical scheme with less detailed labeling. The arrows show the dominant pathway of the actomyosin ATPase activity. (*c*) Simplified four-state biochemical scheme used as a basis for our cross-bridge model.

cycle. All of the states in this main pathway, except the four states shown in boxes, are assumed to be transient intermediates. Therefore the model consists of two unattached (refractory and nonrefractory) and two attached ($AM^{\dagger}\cdot D\cdot P_i$ and $AM^*\cdot D$) cross-bridge states. The arrows in Fig. 1 *a* indicate the directions used in defining the *K*'s.

We can summarize the "evolution" of the actual 4-state cycle that we use in our calculations as follows: (*a*) we start with the 10-state kinetic diagram in Fig. 1 *a* (shown also, with less detailed labeling, in Fig. 1 *b*); (*b*) this is reduced to the single 7-state cycle indicated by the heavy lines in Fig. 1 *a* or by the arrows (dominant direction) in Fig. 1 *b*; and, finally, (*c*) this 7-state cycle is reduced further to a 4-state cycle, as shown by the boxes in Fig. 1 *a* and by Fig. 1 *c*. The alternate notation *R*, *N*, 1, 2 that appears in Fig. 1 will be introduced in section 4.

It should be noted at the outset that reduction of the complete kinetic model shown in Fig. 1 *a* to the four-state cycle shown in Fig. 1 *c* is based on the key assumption (made quantitatively explicit below) that the cross-bridge must dissociate from actin before an ATP molecule is hydrolyzed. This assumption of mandatory dissociation of the cross-bridge-actin

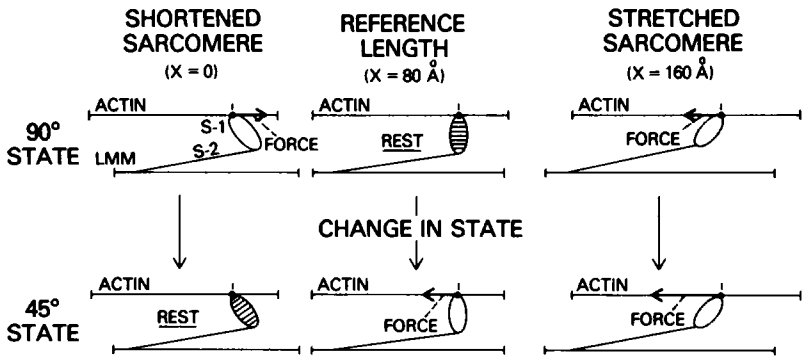

FIGURE 2 Schematic representation of the attached cross-bridge in our model. The 90° and 45° states are shown at three different values of x, the axial position of the actin site to which the cross-bridge is attached. The magnitude and direction of the force exerted by the cross-bridge is indicated by the length and direction of the horizontal arrows along the actin filament. Where the cross-bridge is shaded, it is at its minimum free energy for that state (exerts no force).

complex upon binding of ATP is a key assumption of both the Lymn-Taylor model and the original refractory state model of cross-bridge action (6). Recent biochemical data (see section 11) suggest that, in fact, this assumption may be incorrect; ATP hydrolysis appears to occur in vitro without dissociation of the actomyosin complex. Nevertheless, in the present cross-bridge model, we will still make the simplifying assumption that the binding of ATP causes mandatory dissociation of the cross-bridge-actin complex.

To translate the four-state kinetic cycle shown in Fig. 1 *c* into a complete cross-bridge model, the nature of the attached cross-bridge states must be described. As shown in Fig. 2, we assume in the present model that the attached cross-bridge can exist in two different conformational states (1). In both conformations, the cross-bridge is elastic, that is, as the filaments slide past each other, the cross-bridge exerts either positive or negative force on the actin filament. However, each conformational state has a different optimal attachment angle. In the 90° conformation the cross-bridge exerts zero force when it is attached to actin at a 90° angle, whereas in the 45° conformation the cross-bridge exerts zero force when it is attached at a 45° angle. (These angles are used as convenient generic labels; the exact values could well turn out to be somewhat different.) As shown in Fig. 2, in both conformational states the cross-bridge exerts positive force when it rotates to a larger angle than its optimal angle, and negative force when it rotates to a smaller angle than its optimal angle. In the present model we assume that state $AM^{\dagger}\cdot D\cdot P_i$ is in the 90° conformation, whereas states $AM^{*}\cdot D$, AM, and $AM^{*}\cdot T$ are in the 45° conformation. Thus, at every angle of attachment, state $AM^{*}\cdot D$ exerts a considerably larger force than state $AM^{\dagger}\cdot D\cdot P_i$, and the transition from state $AM^{\dagger}\cdot D\cdot P_i$ to $AM^{*}\cdot D$ causes a marked increase in the force exerted by the cross-bridge (this can be seen quantitatively, below, in Fig. 3 and in Eq. 5).

How does this cross-bridge model differ from that proposed in 1971 by Huxley and Simmons (7)? In both models the cross-bridge is elastic, as was first suggested by A. F. Huxley (8) in 1957. This is, in fact, an essential property of any cross-bridge model. However, it is the relationship of this elasticity to the chemical changes occurring in the cross-bridge that provides the crucial difference between the Huxley-Simmons model and our model. In the Huxley-Simmons model, the elastic element, no matter where it is actually located, is

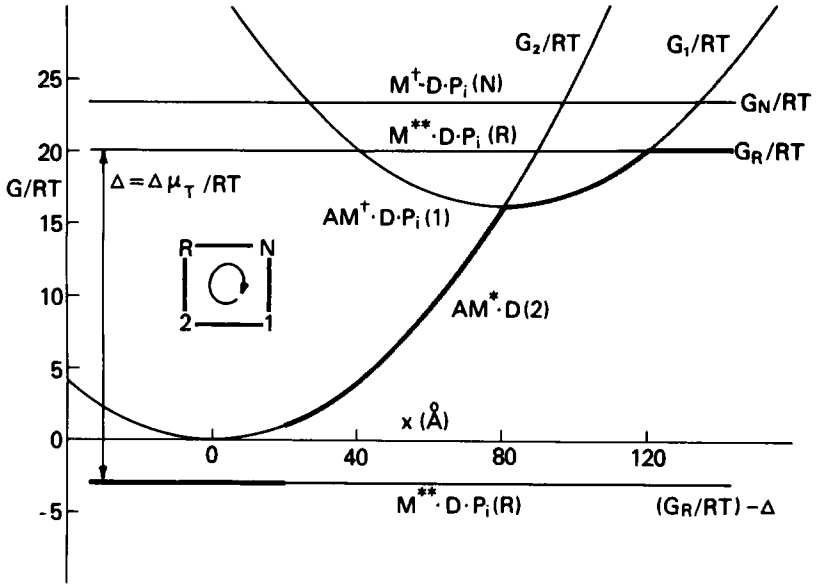

FIGURE 3 Basic free energy profile for our cross-bridge model. The ordinate shows the relative basic free energy/RT for the cross-bridge states (including ATP, ADP, and P_i in solution, as appropriate; see Table I). The minimum basic free energy/RT of the state $AM^* \cdot D$ is arbitrarily set at zero and all other basic free energies are given relative to this value. The abscissa shows the value of x. Δ = chemical potential of ATP hydrolysis, $\Delta\mu_T/RT$.

completely independent of any chemical changes in state occurring elsewhere in the attached cross-bridge. Thus the elastic element must be stretched by one dimensional fluctuations (Brownian motion) before any chemical change in state. This implies (1) that the activation-free energy and, hence, the rates of transition between attached states are strongly related to the positive force produced after the transition, i.e., to the amount the elastic element must be stretched by one dimensional Brownian motion. To make these transition rates realistic, three or more attached states are necessary in the Huxley-Simmons model.

In contrast, we assume (1) that the elasticity and the chemical change in state are intimately tied together. In effect, each of the attached states has its own elastic and chemical properties. Therefore the rate of the transition between the two attached states can be chosen arbitrarily. At the molecular level, two features are required in this kind of model. First, the two attached states should differ by a conformational change in the cross-bridge that affects both the free energy of the attached cross-bridge and the optimal angle of attachment. This conformational change may be localized near the part of the cross-bridge that makes intimate contact with actin on attachment, or it could be more extensive. Second, the conformational change should directly relate the state of the nucleotide at its binding site to the force exerted by the cross-bridge. For example, in Fig. 2, release of P_i should be directly converted into a distortion of the elastic portions of the cross-bridge, without the cross-bridge going over a large free energy barrier, as in the Huxley-Simmons model. There are many detailed molecular changes that could accomplish what is needed; a particular commitment will require more information about the structure of the cross-bridge-actin complex.

3. FREE ENERGY PROFILE

We turn now to the quantitative assumptions we use in our model. Column 2 of Table I gives the in vitro equilibrium constants for all of the transitions shown in the kinetic diagram in Fig. 1 *a*, except K_{13}. No value is given for K_{13} because we assume that $AM^{**} \cdot D \cdot P_i$ does not occur in vivo or in vitro. That is, we assume, first, that k_6 and k_{-6} are negligibly slow so that ATP hydrolysis does not occur when the cross-bridge is attached to actin and, second, that k_{13}, k_{-13}, k_8, and k_{-8} are negligibly slow so that the refractory state is unable to bind to actin. The values in Table I marked with an asterisk are based on experimental data, whereas the three values shown in boxes in column 2 are assumptions we are making in this model. K_9 is then determined as 7.06 M by using 4.71×10^5 M for the equilibrium constant for ATP hydrolysis (19) (3°C, $\Delta G_T^0 = -7.17$ kcal mol^{-1}); the remaining entries in column 2 are then established by exploiting the redundant pathways in the kinetic diagram in Fig. 1 *a* or 1 *b* (biochemists usually refer to this as using "detailed balance").

To convert the horizontal in vitro equilibrium constants in Fig. 1 *a* (equilibrium constants not involving attachment or detachment of actin) to the in vivo equilibrium constants shown in column 3 of Table I, we make a fundamental approximation, used throughout our modeling effort. We assume that the equilibrium constant between any two unattached states or between any two attached states at their minimum free energies are the same in vivo and in vitro. The former assumption (unattached states) is probably very accurate and the latter (see

TABLE I
EQUILIBRIUM CONSTANTS AND FREE ENERGY VALUES IN FIG. 1 *a*

(Ligand)	In vitro	In vivo (at minima)	Basic K (at minima)	Basic ΔG (at minima)
$K_1(T)$	*2.00×10^{10} M^{-1} (9, 10)	‡2.00×10^{10} M^{-1}	6.00×10^7	
$K_2(A)$	*1.00×10^7 M^{-1} (11, 12)	9.95×10^7	9.95×10^7	
$K_3(A)$	1.00×10^{-1} M^{-1}	9.95×10^{-1}	9.95×10^{-1}	
$K_4(T)$	2.00×10^2 M^{-1}	‡2.00×10^2 M^{-1}	6.00×10^{-1}	
K_5	*1.00×10^1 (13, 14, 15)	‡1.00×10^1	1.00×10^1	
K_6K_8	5.48×10^2	‡5.48×10^2	5.48×10^2	
K_7	3.33×10^{-2}	‡3.33×10^{-2}	3.33×10^{-2}	$-1.87\,(RN)$ kcal mol^{-1}
$K_9(P_i)$	7.06 M	‡7.06 M	1.46×10^3	
$K_{10}(P_i)$	4.29×10^4 M	‡4.29×10^4 M	8.89×10^6	8.78 (12)
$K_{11}(D)$	*1.00×10^{-5} M (16, 17)	‡1.00×10^{-5} M	3.33×10^{-1}	
$K_{12}(D)$	*1.00×10^{-4} M (17, 18)	‡1.00×10^{-4} M	3.33	
$K_{14}(A)$	1.65×10^2 M^{-1}	1.64×10^3	1.64×10^3	4.06 ($N1$)
$K_{15}(A)$	1.00×10^6 M^{-1}	9.95×10^6	9.95×10^6	

$\Delta G_T^0 = -RT\ln$ (*4.71×10^5 M) = -7.17 kcal mol^{-1} (19); 3°C. $\Delta\mu_T = RT\ln$ (*9.75×10^9) = 12.63 kcal mol^{-1} (3). [ATP] = *3.00×10^{-3} M (20), [ADP] = *3.00×10^{-5} M (20), $[P_i] = 4.83 \times 10^{-3}$ M (20). $T \equiv$ ATP, $D \equiv$ ADP, $A \equiv$ actin. Although, for consistency, three significant figures are used throughout this table, many of the data values are known much less accurately than this.

*Experimental data values. Box = assumption.

‡Fundamental approximation.

section 11) reasonably accurate (5% in free energy?). By using this approximation we can obtain from column 2 all of the in vivo constants marked with a double dagger in column 3.

In vitro equilibrium constants involving attachment of the S-1 to actin (K_2, K_3, K_{14}, and K_{15}; vertical in Fig. 1 *a*) cannot be converted to in vivo constants without making a further assumption. In vitro, the binding of S-1 to actin is a second-order process whose rate depends on actin concentration. On the other hand, the in vivo attachment of the cross-bridge to actin is a first-order process since a particular cross-bridge, fixed in the myofilament structure, sees only one or a few actin monomers at a time (one, in the present model). Because of this, as indicated by the boxed value of K_2 in column 3 of Table I, we must assume a value for K_2, the first-order binding constant of the nucleotide-free cross-bridge to actin in vivo. Note that K_2 has this value only when the cross-bridge-actin complex is at its minimum free energy, i.e., when the cross-bridge is attached to actin at a 45° angle. Once a value for K_2 in vivo is assumed, the other in vivo binding constants in column 3 of Table I involving attachment of the cross-bridge to actin (K_3, K_{14}, and K_{15}) are found by detailed balance. Note that these equilibrium constants have these values only when the cross-bridge is attached to actin at an angle where it exerts no force (see below): 90° for K_{14} and 45° for K_2, K_3, and K_{15}.

Column 4 of Table I ("basic K") includes the products of the in vivo ligand concentrations (or reciprocals) and the equilibrium constants in column 3 for transitions involving the binding or release of ATP, ADP, or P_i. The other entries in column 4 are the same as in column 3.

The quantity $\Delta\mu_T$ in Table I (bottom), and Eq. 4 below, is the decrease in basic free energy on hydrolysis of ATP, at in vivo ligand concentrations.

To avoid unduly complicated notation, we are using the same symbol K_n in column 1 of Table I (and in the text below) to represent several different kinds of equilibrium constants. In column 2 there are: first-order (isomeric) constants, with no units; second-order binding constants, with units M^{-1}; and second-order dissociation constants, with units M. In column 3 the four actin binding constants are now true first-order constants, with no units. In column 4 the six T, P_i, or D equilibrium constants are now pseudo-first-order constants, with no units. Thus there are two different constants in Table I for each K_n concerned with A, T, P_i, or D. The particular one being referred to in the text (below) can be determined by the context or by the units (M^{-1}, M, or none).

The basic free energy differences between pairs of states at their minimum free energies in vivo is shown in the last column of Table I. These quantities are found from $RT\mathfrak{L}n$ (column 4). It is these differences between pairs of states at their minimum free energies that determine the relative levels of the free energy curves for each of the four states in our cross-bridge model. These free energy curves are presented in the free energy profile shown in Fig. 3 (mathematical details are given later, in section 5). Here the basic free energy of each of the cross-bridge states in vivo is shown as a function of x. The variable x (1–3, 8) is a measure of the position of the actin site relative to the cross-bridge of interest. Because the free energies of the unattached cross-bridge states are independent of the position of the actin site, the free energies of the refractory and nonrefractory states, $M^{**}\cdot D\cdot P_i$ and $M^{\dagger}\cdot D\cdot P_i$, are independent of x. On the other hand, the free energies of the two attached cross-bridge states, $AM^{\dagger}\cdot D\cdot P_i$ (the 90° state) and $AM^{*}\cdot D$ (the 45° state), depend on x. The slope dG_i/dx of a free energy curve for an attached state i, at any value of x, is equal to the force F_i exerted on

the actin filament by the cross bridge in state i, at that x. Of course, F_i is zero where G_i has a minimum.

We now discuss why we chose the minimum levels for the free energy curves shown in Fig. 3 and how these minimum levels are related to the four assumptions (boxed values) made in Table I.

Discussion of Assumptions in Table I

Consider, first, our assumption in Table I that K_2 has a value of $\sim 10^8$ in vivo. This assumption is made for two reasons. The first is to achieve a good thermodynamic efficiency for the model. As can be seen in Fig. 3, we have a free energy change of only 1.65 kcal mol^{-1} in the transition from $AM^* \cdot D$ at 45° to $M^{**} \cdot D \cdot P_i$, that is, in the detachment of the cross-bridge after it has performed its work. This small free energy loss is necessary to keep the efficiency high. Because this free energy change is 1.65 kcal mol^{-1}, $K_{12}K_4K_5/K_3$ must equal 20.1. Furthermore, because experimental data (Table I) show that K_{12} is 3.33 and K_5 is 10.0 in vivo, it follows that K_4/K_3 must be 0.603 in vivo. By detailed balance we then deduce that K_1/K_2 must also equal 0.603 in vivo. Because there is experimental evidence that $K_1 = 6.00 \times 10^7$ in vivo, it follows that we must assume that $K_2 = 9.95 \times 10^7$ in vivo, as shown in Table I. Thus, to obtain a good efficiency for the model, the binding constant of the cross-bridge to actin at 45° in vivo (basic K_2 in Table I) must be assumed to be approximately equal to the binding constant of ATP to myosin in vivo (basic K_1 in Table I). It has, in fact, generally been recognized that the strength of binding of ATP and actin to myosin in vivo should be about the same (1, 21, 22).

Our assumption that K_2 in vivo is $\sim 10^8$ implies that the binding constant of the cross-bridge to actin at 45° in vivo is equal to the effective binding constant of S-1 to actin in vitro when the actin concentration is ~ 10 M (see K_2, column 2), an extremely high actin concentration which is of course unobtainable. By the same argument, if we assumed that the binding constant of the cross-bridge to actin at 45° in vivo were equivalent to the effective binding constant in vitro when the actin concentration was, say, 1×10^{-3}M, then the binding constant in vivo would be $K_2 \simeq 10^4$. This would be 10^4 lower than the binding constant of ATP to myosin in vivo, which would make the free energy drop on detachment of the cross-bridge in our model 6.7 kcal mol^{-1}. Thus our cross-bridge model would be quite inefficient.

The second reason for assuming that K_2 has a value of $\sim 10^8$ in vivo is to make K_{15}, the binding constant of $M^* \cdot D$ to actin at $x = 0$, have a value of $\sim 10^7$. K_{15} is determined indirectly by K_2 because experimental data (17) show that K_{11}/K_{12} is ~ 0.1 and, by detailed balance, $K_{11}/K_{12} = K_{15}/K_2$. The reason it is important that K_{15} have a value of $\sim 10^7$ or more is related to the fact that the free energy curves for $AM^{\dagger} \cdot D \cdot P_i$ and $AM^* \cdot D$ intersect at $x = 80$ Å (Fig. 3); hence, at and just less than $x = 80$ Å, $AM^* \cdot D$ is the major force-producing state in our model. If K_{15} were $< 10^7$, $M^* \cdot D$ would be more stable than $AM^* \cdot D$ at x 80 Å, and the cross-bridge would detach at this x, with loss of force production. Therefore we require: $K_{15} \geq K_{10} = 9 \times 10^6$.

Note that our assumption of a value of $\sim 10^8$ for K_2 may have implications for the rate of attachment of the cross-bridge to actin at a 45° angle in the absence of nucleotide. If the rate constants for detachment of the cross-bridge from actin at $x = 0$ in vivo were similar to the rate constant for detachment of S-1 from actin in vitro, ~ 0.1 s^{-1} (23), then the rate constant

for attachment of the cross-bridge to action in vivo at $x = 0$ would have to be $\sim 10^7\ s^{-1}$. This, of course, is a very high rate of attachment.

The second assumption we make in Table I is that $K_3 = 1 \times 10^{-1}\ M^{-1}$ in vitro and therefore, by detailed balance, $K_3 \simeq 1$ in vivo at $x = 0$. The rate of the transition from $AM^* \cdot T$ to $M^{**} \cdot D \cdot P_i$ at $x = 0$ is $\simeq k_5/(1 + K_3)$ (assuming a fast equilibrium between $M^* \cdot T$ and $AM^* \cdot T$) (24). Clearly, the larger K_3, the slower the cross-bridge will detach after it reaches 45°. To keep this rate reasonably fast, we have made $K_3 \simeq 1$ in vivo at $x = 0$.

Note that already this model has made two specific biochemical predictions that can be tested experimentally. First, we have introduced the value K_3 (in vitro) $= 1 \times 10^{-1}\ M^{-1}$. Thus, unless the actin concentration approaches 10 M, $M^* \cdot T$ should not bind to actin in solution. Second, by detailed balance, the model predicts that K_4, the binding constant of ATP to actomyosin, in vitro, is $2 \times 10^2\ M^{-1}$. We do not mention these predictions to imply that they are verified by current experimental data (see section 11) but only to emphasize the relationship between cross-bridge behavior in vivo and biochemical data in vitro.

The third assumption we make is that $K_7 = 3.33 \times 10^{-2}$ in vitro, that is, the equilibrium between the refractory and nonrefractory states is shifted toward the refractory state. As will be seen below, this guarantees that during isotonic contraction the cross-bridge must make the rate-limiting transition from the refractory to the nonrefractory state before the cross-bridge can attach to actin. This in turn limits the rate of ATP hydrolysis at high velocities of contraction.

Our fourth assumption about the equilibrium constants is that $K_{14} = 1.65 \times 10^2 M^{-1}$ in vitro. By detailed balance (in column 3) it then follows that $K_{14} = 1.64 \times 10^3$ in vivo, which in turn implies that $K_7 K_{14} \simeq 55$ in vivo. In effect, $K_7 K_{14}$ is the equilibrium constant between $M^{**} \cdot D \cdot P_i$ and $AM^{\dagger} \cdot D \cdot P_i$ at $\times = 80$ Å. Therefore, the value of $K_7 K_{14}$ determines the fractions of cross-bridges in states $AM^{\dagger} \cdot D \cdot P_i$ and $M^{**} \cdot D \cdot P_i$, in the isometric state, at $x > 80$ Å. For example, if we assumed $K_7 K_{14}$ in vivo were equal to 1, almost no cross-bridges would be attached to actin in the isometric state, at $x > 80$ Å; they would be in the refractory state. As we will explain in Section 7, this would make it almost impossible for the model to fit the experimental T_1 and T_2 curves of the isometric transient (14). For this reason we assumed that $K_{14} = 1.65 \times 10^2\ M^{-1}$ in vitro.

Assuming a value for K_{14} in vitro leads to another biochemical prediction. As we shall show below, K_{14} is a key determinant of the value of K_{app} that is obtained experimentally from a double reciprocal plot of ATPase rate vs. actin concentration.

Further Assumptions of the Model

The equilibrium constants between states shown in Table I establish only the relative levels of the free energy curves in Fig. 3. Further assumptions are required to specify the free energy profile completely. First, we assume that each cross-bridge can interact with only one actin monomer per repeat of the actin helix, i.e., per 360 Å (this is a "single-site" model). This single-site assumption is very likely incorrect because the azimuthal flexibility of the cross-bridge will probably allow it to interact with several adjacent actin monomers along the actin filament. However, we are making this assumption in the present paper to keep the model simple. If a cross-bridge could interact with several actin monomers along the thin filament, a separate set of free energy curves (for attached states) would have to be included

for each actin monomer (25). Note that since we assume that only one actin monomer is available with which a cross-bridge can interact, it follows that, in this model, only one cross-bridge head at a time can interact with actin.

In future work we plan to use multiple actin sites and also, in place of 360 Å, a repeat distance of $7 \times 55 = 385$ Å.

To complete the free energy profile shown in Fig. 3, we also assume that the two attached states have parabolic free energy curves with the same curvature (force constant). In addition, we assume that the two parabolas intersect at the point where the 90° state has its minimum free energy. Finally, we have chosen 80 Å as the distance between free energy minima of the two attached states to obtain $T_1 = 0$ (4) for a release of ~40 Å (26) (see section 7).

The assignment (section 2) of the approximate angles 90° and 45° to the two attached states, with free energy minima separated by 80 Å, implies something about the length of S-1. But at the present time this length and both angles are not known with great accuracy, so it is difficult to check the 80-Å figure for self-consistency. Nevertheless, it is probably not an unreasonable choice (1).

4. VALUES OF THE INDIVIDUAL RATE CONSTANTS

Thus far in this paper we have discussed the equilibrium assumptions required to convert the kinetic model, shown in Fig. 1 *c*, into the free energy profile, shown in Fig. 3, but we have not yet specified the individual rate constants as functions of x. Our assumed functions for these first-order rate constants are shown in Fig. 4. This figure introduces new simplified notation to describe the four states in our model: $R = M^{**} \cdot D \cdot P_i$ (refractory state); $N = M^{\dagger} \cdot D \cdot P_i$ (nonrefractory state); $1 = AM^{\dagger} \cdot D \cdot P_i$ (90° state); $2 = AM^{*} \cdot D$ (45° state). For each of the four pairs of in vivo transitions in our model, $R \rightleftharpoons N$, $N \rightleftharpoons 1$, $1 \rightleftharpoons 2$, and $2 \rightleftharpoons R$, we can then define a set of in vivo first-order rate constants: α_{RN}, α_{NR}; α_{N1}, α_{1N}; α_{12}, α_{21}; and α_{2R}, α_{R2}, respectively. In general, the values of these in vivo rate constants are functions of x; the in vitro rate constants, of course, are not functions of x.

For in vitro rate constants, we shall use the notation $k_i/k_{-i} = K_i$. For example, for the in vitro transition between R and N, the forward and reverse rate constants are k_7 and k_{-7}, respectively. The relationship between the values of the in vitro and in vivo rate constants will be discussed below.

For each of the four pairs in vivo transitions, once we assume a value for either the forward or reverse rate constant at a given value of x, the other rate constant is determined. This is because the free energy curves in Fig. 3 specify the in vivo equilibrium constants, α_{ij}/α_{ji}, between any two states i and j at a given value of x. Note that the equilibrium constants given in column 4 of Table I are always between the minimum free energies of the in vivo states. Therefore only in special cases are they equal to α_{ij}/α_{ji} at a particular value of x. For example, $K_7 = \alpha_{RN}/\alpha_{NR}$ at all values of x, $K_{14} = \alpha_{N1}/\alpha_{1N}$ at $x = 80$ Å, and $K_{10} = \alpha_{12}/\alpha_{21}$ at $x = 40$ Å.

Before going into details about the rate constants, two general comments may be helpful. First, because the calculated isometric transients occur on a very fast time scale (4), they are virtually unaffected by several rate constants to which the force-velocity curve is very sensitive. Therefore we were able to use two of the eight rate constants (α_{12} and α_{21}) to fit the isometric transient data and then use the other rate constants to fit the force-velocity curve

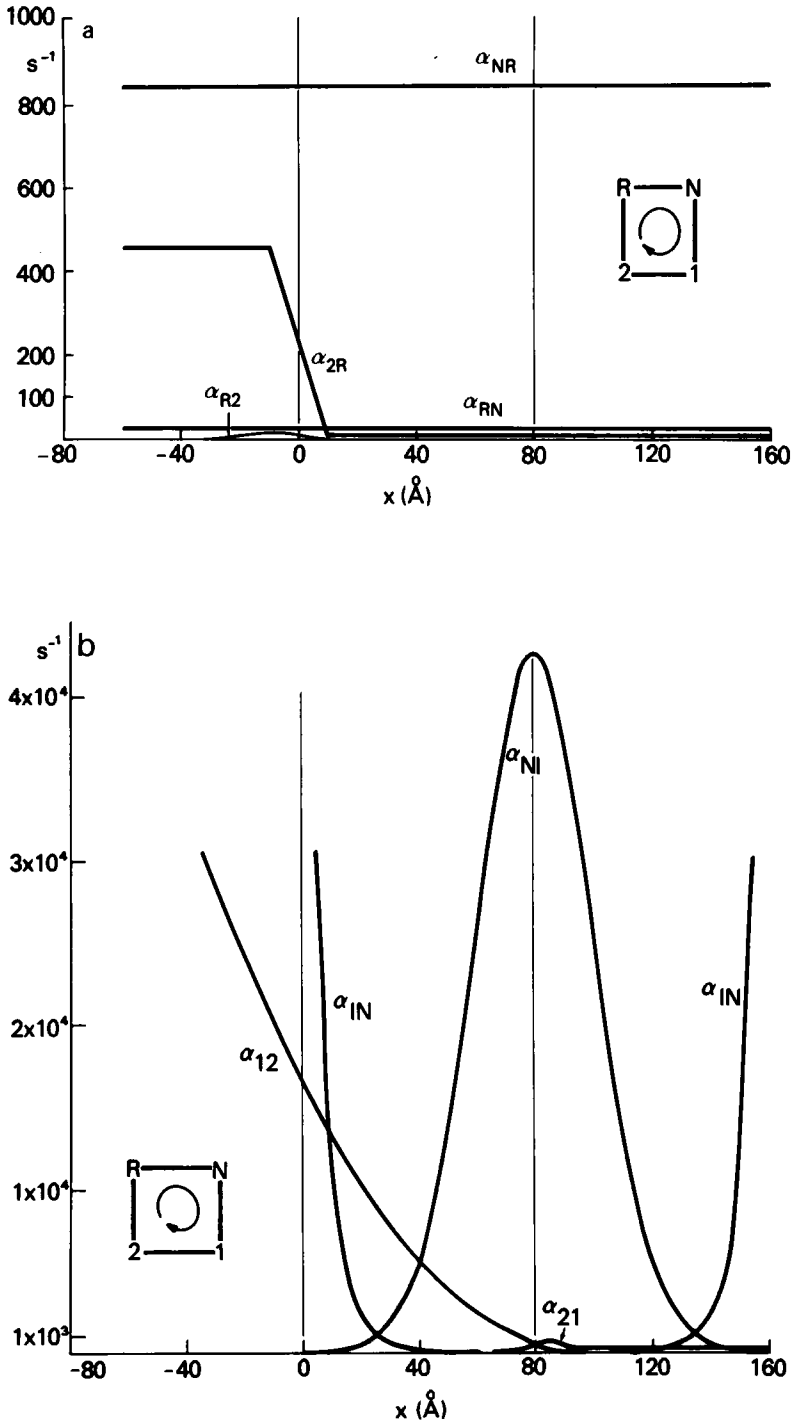

FIGURE 4 The first-order rate constants for the transitions between the cross-bridge states as a function of x, in our model.

(see sections 7 and 8 for details). Second, during the course of this work we calculated the properties of our model with ~20 different sets of rate constant choices. The discussion below relates to our final rate constant selection. Improved agreement with experimental data could have been achieved by further minor alterations of the rate constants, but in our judgment this would have gone beyond the point of diminishing returns for this type of model.

Our first specific rate constant assumption is a value of 28.1 s^{-1} for α_{RN}, the constant for the rate-limiting transition from R to N. Since $\alpha_{RN}/\alpha_{NR} = K_7 = 3.33 \times 10^{-2}$ (Table I and Fig. 3), α_{NR} then has a value of 842 s^{-1}. Because the value of α_{RN} effectively determines the rate of attachment of the cross-bridge to actin, it is of crucial importance in determining the force-velocity curve. Note that 28.1 s^{-1} is the value of α_{RN} for a cross-bridge with two heads. This rate constant per cross-bridge head or for S-1 would be 14 s^{-1}.

We next assume that α_{N1}, the actual attachment rate of the cross-bridge to actin, is very large, with a value of 4.26×10^4 s^{-1} at $x = 80$ Å, where the cross-bridge attaches to actin at a 90° angle. We further assume that this rate constant decreases as the angle of attachment either increases or decreases; concomitantly, the reverse rate constant α_{1N} increases. Other than assuming that α_{N1} is large near $x = 80$ Å and α_{1N} is large near $x = 0$ and 160 Å, the exact values of these rate constants are not crucial. The decrease in α_{N1} for x below 30 Å does have an effect on the probability of state 1 (the 90° state) in the isometric state. But in fact both α_{N1} and α_{1N} could be increased greatly without having a marked effect on calculated properties.

The third set of rate constants in our four-state model is α_{12} and α_{21}, the rate constants for the transitions between states 1 (90°) and 2 (45°); state 2 is the major force-producing state. At $x = 80$ Å, where both the 90° and 45° states are at 90° and have the same free energy, $\alpha_{12} = \alpha_{21} = 438$ s^{-1}. This value of these rate constants and their x dependence have been chosen to give a suitable rate of force recovery in isometric transients (see section 5).

The fourth transition in our four-state model is the overall transition from the major force-producing state 2 back to state R. As can be seen in Fig. 1 *a*, this overall transition involves a number of different steps: ADP release, rebinding of ATP, detachment from actin, and the initial P_i burst. Thus, at $x = 0$, $\alpha_{2R}/\alpha_{R2} = K_{12}K_4K_5/K_3$, where these equilibrium constants are taken from column 4 of Table I. In the present model we assume that the rebinding of ATP, detachment from actin, and the initial P_i burst are rapid compared to the rate of ADP release so that $AM^* \cdot D$ (state 2) is the only 45° state that occurs to a significant extent in vivo. This assumption also implies that α_{2R} is essentially a measure of the rate of ADP release in vivo (but α_{R2} is not the rate constant for ADP binding).

As can be seen in Fig. 4 *b*, we assume that the value of α_{2R} has a very specific dependence on x. At values of $x > 10$ Å, i.e., where state 2 (45°) is at an angle > 45° and is thus exerting positive force, α_{2R} is very small. We assume it has a value of only 8.77 s^{-1}, approximately one-third the value of α_{RN}. Since α_{RN} determines the rate of attachment of the cross-bridge, whereas α_{2R} determines its rate of detachment, by making α_{2R} less than α_{RN} in the region where the cross-bridge exerts positive force, we make certain that the cross-bridge is usually attached in this region. On the other hand, at values of $x < -10$ Å, where state 2 is at an angle <45° and is therefore exerting considerable negative force, we assume $\alpha_{2R} = 456$ s^{-1}. Here the cross-bridge detaches quite rapidly. The basic assumption that the cross-bridge detaches slowly where it exerts positive force but very rapidly where it exerts negative force was first proposed by A. F. Huxley in 1957 (8). It is difficult to imagine a cross-bridge model without

this assumption but, as yet, there is no in vitro evidence for it. In our model, the origin of the x dependence of α_{2R} lies in the detailed molecular structure of state 2 as its angle with actin changes. Such a structural alteration could easily affect the rate of ADP release. Note again the intimate relationship between the elasticity of the cross-bridge and its chemical behavior in our model.

5. SOME DETAILS OF THE CALCULATIONS

In this section we digress to give a few mathematical details. We use notation that is convenient for this purpose. The basic free energy functions in Fig. 3 are:

$$G_N/RT = 23.401, \quad G_R/RT = 20.000, \tag{1}$$

$$G_1/RT = 16.000 + [(x - 80)^2/2\sigma^2], \tag{2}$$

$$G_2/RT = x^2/2\sigma^2, \tag{3}$$

$$\Delta \equiv \Delta\mu_T/RT = 23.000, \tag{4}$$

where x is in Å and $\sigma^2 = 200$ Å^2. The force functions for the two attached states are then:

$$F_1\sigma^2/RT = x - 80, F_2\sigma^2/RT = x. \tag{5}$$

The final first-order rate constants used (Fig. 4), which must be consistent with the free energy functions, are as follows:

$$\alpha_{RN} = 28.06s^{-1}, \alpha_{NR} = 841.9s^{-1}, \alpha_{NR}/\alpha_{RN} = 30 \tag{6}$$

$$\alpha_{N1} = 1052.4 \exp [(G_N - G_1)/2RT]\ s^{-1} \tag{7}$$

$$\alpha_{1N} = 1052.4 \exp [(G_1 - G_N)/2RT]\ s^{-1}. \tag{8}$$

Thus α_{N1} is a Gaussian function and α_{1N} is a reciprocal Gaussian. The free energy difference $G_N - G_1$ is "split" evenly between the two rate constants. (Attachment is a first-order process here; it is not a diffusion-controlled, second-order process as it is in solution.)

The rate constant α_{2R} is taken as a step function with a nonvertical step (Fig. 4 *b*):

$$\begin{aligned} \alpha_{2R} &= 456.0\ \text{s}^{-1}\ (x \leq -10\ \text{Å}) \\ &= 8.77\ \text{s}^{-1}\ (x \geq 10\ \text{Å}) \\ &= 228.0 - 22.8x\ \text{s}^{-1}\ (-10\ \text{Å} < x < 10\ \text{Å}). \end{aligned} \tag{9}$$

Then α_{R2} (Fig. 4 *b*) is determined by

$$\alpha_{2R}/\alpha_{R2} = \exp [(G_2 - G_R + \Delta RT)/RT]. \tag{10}$$

The α_{12} curve in Fig. 4 *a* cannot be represented by an analytical expression. Except for minor modifications, we obtained the shape of $\alpha_{12}(x)$, relative to $\alpha_{12}(0)$, by: (*a*) starting with the shape of the Ford-Huxley-Simmons (FHS) (4) $t_{1/2}^{-1}$ curve in Fig. 8; (*b*) making simplifying assumptions about the state probability distributions (26); and (*c*) solving numerically an integral equation in $\alpha_{12}\ (x)$ that relates $\alpha_{12}\ (x)$ to the averaged (over x) quantity, $t_{1/2}^{-1}(y)$, where y is the step length in an isometric transient. The determination of the absolute magnitude of $\alpha_{12}\ (x)$ (and the other rate constants) will be discussed in sections 7 and 8.

Fig. 4 *a* shows $\alpha_{21}(x)$ also. The small peak in α_{21} at $x = 85$ Å was found necessary to make $t_{1/2}^{-1}$ in Fig. 8 continuous in slope at $y = 0$. These two rate constants are related by:

$$\alpha_{12}/\alpha_{21} = \exp[(G_1 - G_2)/RT]. \tag{11}$$

The general computational procedure (see reference 2, 110–117, or reference 3, 284–291) is to solve an appropriate set of differential equations in the state probabilities $p_i(x, t)$ or $p_i(x; v)$, where $i = R, N, 1, 2$, and then to calculate the mean force F or flux J from:

$$\bar{F} = (1/d) \int_{-d/2}^{+d/2} [p_1(x)F_1(x) + p_2(x)F_2(x)]dx \tag{12}$$

$$\bar{J} = (1/d) \int_{-d/2}^{+d/2} [\alpha_{RN} p_R(x) - \alpha_{NR} p_N(x)]dx, \tag{13}$$

where d is the repeat distance, 360 Å. The flux equation is used only under steady conditions; any one of the other three transition pairs ($N1$, 12, $2R$) could also be used as the integrand (2, 3).

The efficiency η, in a steady contraction at velocity v, is (2, 3):

$$\eta = \bar{F}v/\bar{J}\Delta\mu_T. \tag{14}$$

The mean number of completed cycles per pass of an actin site past a given cross-bridge is $r = Jd/v$ (3, 27).

The differential equations applicable to the isometric transients were solved for the $p_i(t)$, at 5 Å intervals in x, using the standard matrix method. These are linear first-order equations with constant coefficients. The same interval was then used in the numerical integration of Eq. 12 to obtain $F(t)$. For a steady contraction at a given v, the differential equations were solved by starting with the known solution (R and N at equilibrium) at large positive x and then extending the solution, step-by-step and numerically, to large negative x, using finite steps on the x axis adjusted in size to the velocity (except for a region of analytical integration at the end of the process). Then $\bar{F}(v)$ and $\bar{J}(v)$ were obtained from Eqs. 12 and 13 using numerical integration with 5-Å intervals in x.

6. DOUBLE RECIPROCAL PLOT OF ATPASE RATE VS. ACTIN CONCENTRATION

The free energy profile in Fig. 3 combined with the rate constant assumptions in Fig. 4 can now be used to fit the steady-state and presteady-state physiological data (4, 28, 29) obtained from frog muscle at 3°C (sections 7 and 8). However, it is of interest to examine first an important biochemical prediction that can be made from our rate constant assumptions. We made the fundamental approximation, above, that equilibrium constants between states at their minimum free energies are the same in vivo as in vitro. This approximation can be extended to individual rate constants by assuming that the in vitro rate constant for a transition from a state of higher minimum free energy to a state of lower minimum free energy is equal to the in vivo rate constant for this transition at the point where the state of higher minimum free energy is at its minimum free energy. For example, in this approximation, k_{10} in vitro would be equal to α_{12} in vivo at $x = 80$ Å, where state 1 is at its minimum free energy. The value of k_{-10} in vitro would then be approximated by k_{10}/K_{10}. On the same basis, k_7 and k_{-7} in vitro would be equal to α_{RN} and α_{NR} in vivo, respectively. Of course, as with equilibrium constants (see section 3), this assumption does not apply to the rate of attachment of the cross-bridge to actin.

This approximation is probably accurate for k_7 and k_{-7}. However, it is presumably

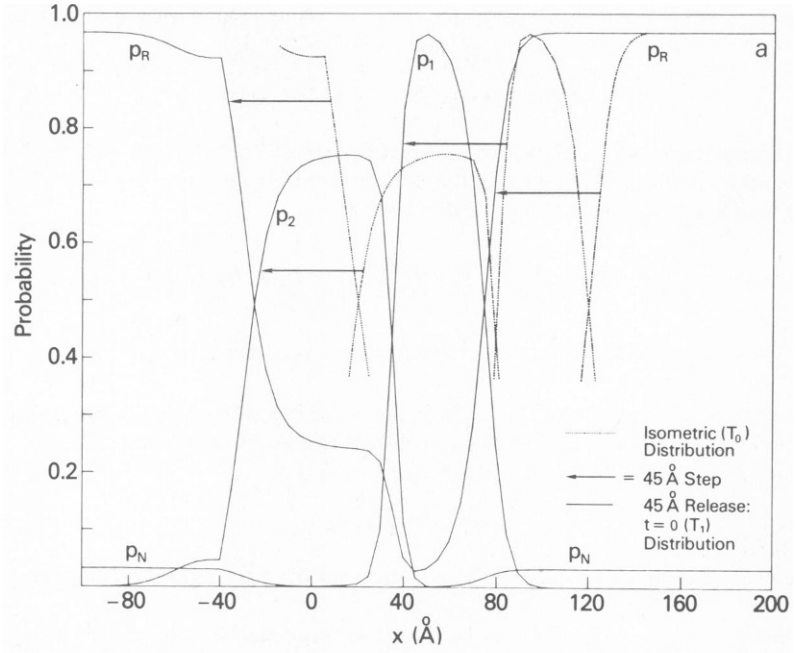
1.0
0.8
0.6
0.4
0.2
Probability
p_R
p_1
p_R
a
p_2
Isometric (T_0) Distribution
= 45 Å Step
45 Å Release: t = 0 (T_1) Distribution
p_N
p_N
−80
−40
0
40
80
120
160
200
x (Å)

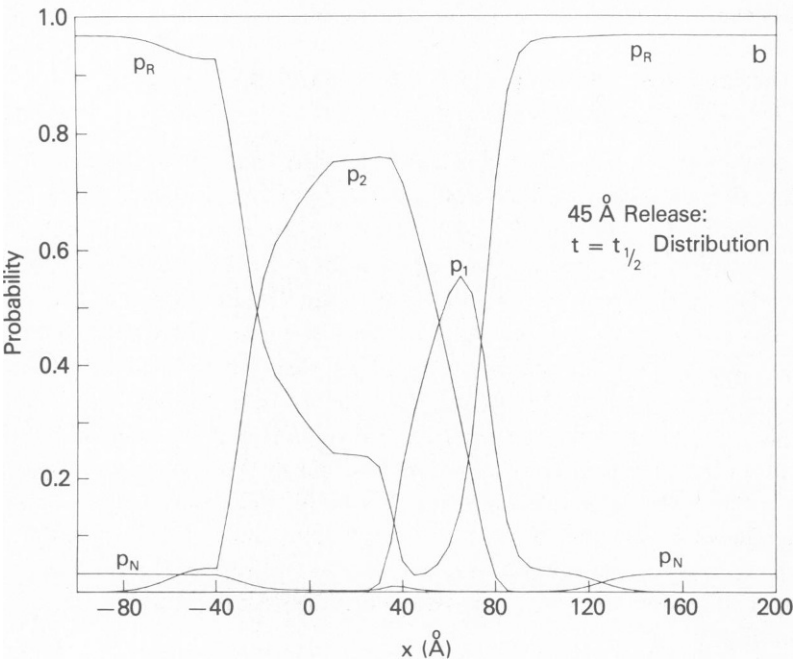
1.0
0.8
0.6
0.4
0.2
Probability
p_R
p_R
b
p_2
45 Å Release:
$t = t_{1/2}$ Distribution
p_1
p_N
p_N
−80
−40
0
40
80
120
160
200
x (Å)

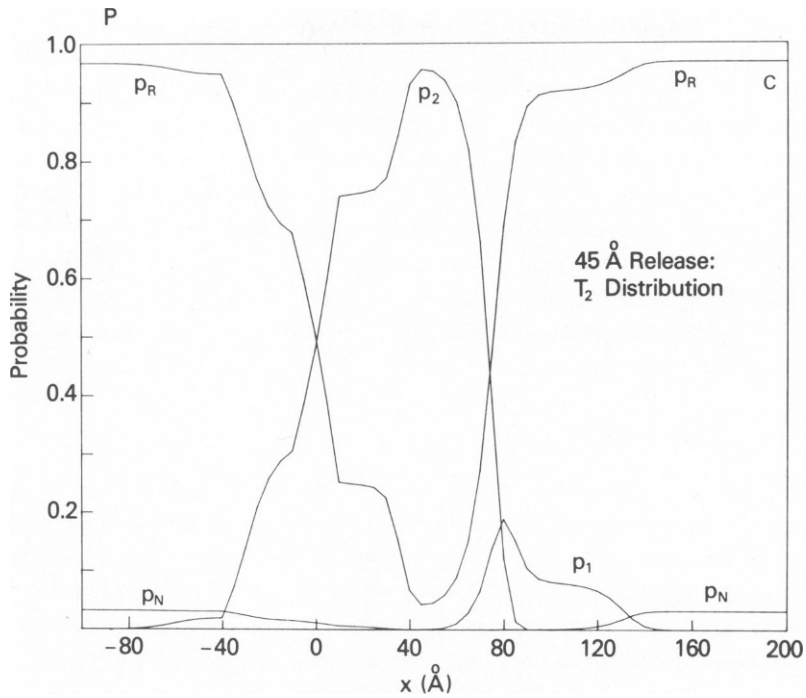

FIGURE 5 The probability distribution of the cross-bridge states calculated from our model, as a function of x, in the isometric state and at various times after a 45-Å release. (*a*) The isometric distribution, T_0 (dotted curves), and the distribution after a 45-Å release, T_1 (solid curves), are identical except for a shift of 45-Å on the abscissa. (*b*) Distribution when the force has recovered one-half of the way to its T_2 value. (*c*) Distribution when the force has recovered to its T_2 value (see text for description of how T_2 is defined).

somewhat in error for k_{10}: in moving on the free energy surface from state 1 to state 2 (see Fig. 6 of reference 1), a lower saddle point is available in vitro than in vivo because x is constrained to be constant in vivo, but not in vitro. Thus we would expect k_{10} (in vitro) $> \alpha_{12}$ (in vivo) at $x = 80$ Å.

Nevertheless, on the basis of this approximation, we can use the in vivo rate constants shown in Fig. 4 to make a rough prediction of a double reciprocal plot of ATPase rate vs. actin concentration in vitro (30). Provided k_5 is not rate limiting and $K_3 = 1 \times 10^{-1}\text{M}^{-1}$, as was assumed earlier, it can easily be shown that, on the basis of Fig. 1 *a*, a linear double reciprocal plot should be obtained with $V_{max} = k_7$ and $K_{app} = k_{-7}/k_{10}K_{14}$. (Note that we used the symbol V_{max} for the maximum actin-activated ATPase rate in vitro and the symbol v_m, below, for the maximum velocity in the force-velocity curve.) Therefore, $V_{max} = 28\ \text{s}^{-1}$ per two myosin heads or $14\ \text{s}^{-1}$ per S-1 because $k_7 = \alpha_{RN} = 28\ \text{s}^{-1}$ (Fig. 4). Likewise, $K_{app} = 1.16 \times 10^{-2}\text{M}$ because $k_{-7} = \alpha_{NR} = 842\ \text{s}^{-1}$ (Fig. 4), $k_{10} = \alpha_{12} = 438\ \text{s}^{-1}$ at $x = 80$ Å (Fig. 4), and $K_{14} = 1.65 \times 10^{2}\text{M}^{-1}$ (column 1, Table I).

How do these values compare with experimentally obtained values for V_{max} and K_{app}? Only one biochemical study on frog myosin has been reported, and in this study denaturation was a major problem because the myosin lost 25% of its activity each day (31). Thus a large

correction had to be applied to the S-1 data. No reciprocal plot could be obtained but the authors reported a V_{max} of 4.5 s^{-1} per S-1 at 1°C. This is approximately one-third the value we are using for $k_7 = V_{max}$ (per S-1). However, in view of the large correction that had to be applied for denaturation, our value of 14 s^{-1} per S-1 does not seem to be unreasonable. As will be seen below, we chose this value to obtain a realistic force-velocity curve.

The value for K_{app} predicted by our model does not agree as well with experimental data. No value for K_{app} was reported with frog S-1 but with rabbit S-1 at 0°c, at very low ionic strength, $K_{app} \simeq 10^{-5}$ M (32), and at 50 mM ionic strength, $K_{app} \simeq 10^{-4}$ M (33). Assuming a further increase in K_{app} with increasing ionic strength, an experimental value of $\sim 5 \times 10^{-4}$ M for K_{app} at 0.15 M ionic strength seems likely. The value of 1.2×10^{-2} M estimated from our model for K_{app} therefore appears to be too large.

7. ISOMETRIC TRANSIENTS

We next examine how our model fits the isometric transient data (4) obtained with frog muscle at 3°C. In attempting to fit these data, we assume that the experimental phenomena observed are all due to cross-bridge behavior. That is, we assume that all of the elasticity shown by active muscle resides not in a series elasticity, e.g., the thin filaments, but in the cross-bridges themselves (7). If there were a considerable amount of series elasticity, it would make interpretation of the isometric transient data much more complex (25). Correspondingly, we make the usual assumption that no significant motion of the filaments takes place in the isometric state.

The calculated isometric distribution of cross-bridges, $p_i(x)$, is shown as the dotted curves in Fig. 5 *a*. The more detailed solid curves are identical, but are shifted by 45 Å (see below). This same isometric distribution is shown as the dashed curves in Fig. 11 *a*, and is also indicated schematically by the heavy solid lines in Fig. 3. As can be seen for $x > 80$ Å, i.e., at angles of attachment >90°, most of the cross-bridges are attached in state 1 (90° state), whereas for $x < 80$ Å, most of the cross-bridges are attached in state 2 (45° state), the major force-producing state. The reason for this is obvious from the free energy profile in Fig. 3 where, for $x > 80$ Å, the free energy of state 1 is markedly lower than the free energy of state 2, whereas for $x < 80$ Å the opposite is the case.

What determines the range over which the cross-bridges are attached? For cross-bridges attached at angles >90° ($x > 80$ Å), the free energy of state 2 is so much higher than the free energy of state 1 that almost no cross-bridges make the transition from state 1 to state 2. Thus the cross-bridges attached at angles >90° do not cycle and hydrolyze ATP to a significant extent. Rather, an equilibrium occurs between states R and 1 and a simple Boltzmann distribution determines the range over which the cross-bridge is attached. As shown in Fig. 3, for $x > 120$ Å the equilibrium shifts toward state R and very few cross-bridges are attached.

Cross-bridges attached at angles <90° ($x < 80$ Å) do cycle and hydrolyze ATP because state 2 is at a lower free energy than state 1. Here the distribution of attached cross-bridges is determined by the relative rates at which cross-bridges enter and leave state 2. Because α_{12} is very large, the effective rate constant with which they enter state 2 is $\alpha_{RN}\alpha_{N1}/(\alpha_{N1} + \alpha_{NR})$, whereas the rate constant with which they leave state 2 is α_{2R} (see Fig. 1 *a*). So long as $\alpha_{N1} \gg \alpha_{NR}$, the entering rate constant is α_{RN} (28 s^{-1}), whereas the departing rate constant is $\alpha_{2R} = 8.8$ s^{-1}. Thus, between $x = 20$ and 80 Å, most of the cross-bridges are attached and in

state 2. For $x < 20$ Å, $\alpha_{N1} < \alpha_{NR}$ and thus the number of cross-bridges attached in state 2 decreases markedly.

Fig. 6 shows the time-courses of force changes calculated from our model after releases or stretches of various lengths y. These isometric transients are quite similar to the experimental transients observed by FHS. After an instantaneous increase or decrease in force, the force rapidly returns almost to its original level. As indicated at the bottom of Fig. 6, the "early" isometric transient is partially characterized by two parameters: T_1, the level the force reaches immediately after the change in length; and T_2, the level to which the force first recovers (4).

As is clear from FHS, the location of the experimental T_2 level is somewhat arbitrary. We used the following procedure, which is also arbitrary. In the computer print-out for a given y, either $p_1(t)$ or $p_2(t)$ passes through a maximum as t increases from $t = 0$ whereas the other passes through a minimum. The time at which the second of these two extrema occurs (whether maximum or minimum) is taken as the T_2 point, i.e., taken to be the conclusion of the first (fast) phase of the transient. We made no attempt in this model to fit the later portion of the isometric transient that occurs after T_2. At the present time the experimental data for this slower portion of the transient is somewhat variable (4), which is why, even experimentally, it has been difficult to define the T_2 level.

Fig. 5 *a–c* show the change in cross-bridge distribution that occurs during an isometric transient after a 45-Å release. Immediately after the release, in which x is decreased by 45 Å,

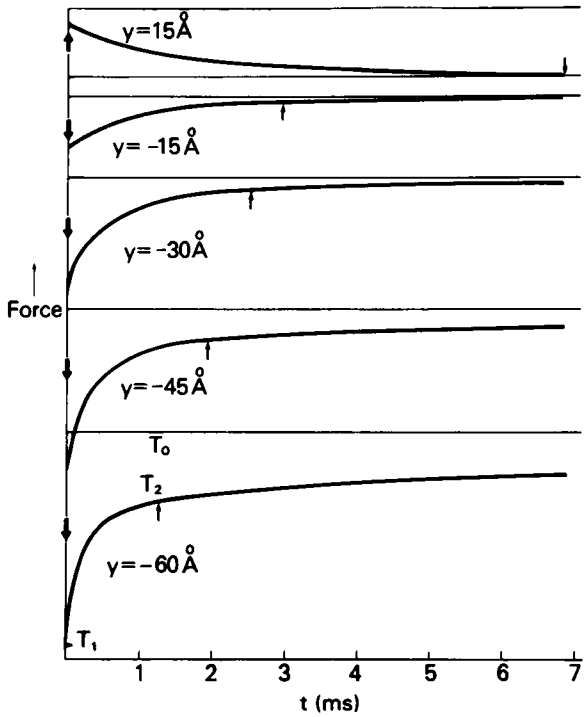

FIGURE 6 Change in force, calculated from our model, as a function of time after a sudden stretch or release. The thick arrows on the ordinate show the direction of the force change during the stretch or release. The small arrows show the points defined as T_2 in our model for end of the transients (see text). y – magnitude of the sudden stretch or release.

TABLE II
FRACTION OF ATTACHED CROSS-BRIDGES AT T_2

y	p_1	p_2	$p_1 + p_2$
Å			
−60	0.011	0.197	0.208
−45	0.018	0.196	0.214
−30	0.041	0.186	0.227
−15	0.075	0.165	0.240
− 5	0.097	0.145	0.242
0 (T_0)	0.106	0.135	0.241
+ 5	0.112	0.125	0.237
+15	0.113	0.111	0.224

all of the attached cross-bridges have been forced to rotate to angles at which they exert less force than in the isometric state (Eq. 5 shows that both F_1 and F_2, the forces exerted by the 90° and 45° states, respectively, decrease if x is decreased). This is shown in Fig. 5 *a*, where the isometric distribution (dotted curves) has been shifted to the left 45 Å (solid curves, T_1 distribution) but otherwise not altered. In our model the recovery of force then occurs as cross-bridges at angles <90° (x < 80 Å) transform from state 1 where they exert negative force to state 2, where they exert positive force. This change in state can be seen in Figs. 5 *b* ($t = t_{1/2}$, the time to half-recovery to T_2) and *c* (t = time at which T_2 is reached).

Note that few cross-bridges attach or detach during the early transient. Almost all of the change in force is due to the transition from the 90° state to the 45° state. In a stretch transient, the same is true except that here the 45° state transforms to the 90° state.

Table II confirms that with this model there is little change in the number of attached cross-bridges during the early transient (the T_0 or Y_0 value of $p_1 + p_2$ is the starting value in all cases). This feature of the model was chosen to agree with the experimental data of Huxley and Simmons (34), which indicated that almost no change in stiffness occurs during the transient. Since stiffness should be proportional to the number of attached cross-bridges (assuming there is very little series elasticity) these data suggested, first, that there is no significant difference between the number of cross-bridges attached in the isometric state and the number attached at the T_2 level and, second, that all attached cross-bridge states have the same stiffness. By making the force constants of states 1 and 2 identical, we guarantee that no change in stiffness occurs as attached cross-bridges change state.

Fig. 7 shows the calculated T_1 and T_2 as functions of the magnitude of the release or stretch (y). For comparison, the FHS experimental values are also shown. As can be seen, the theoretical T_1 and T_2 curves are quite similar to the experimental curves except that, at large releases, the theoretical T_2 curve decreases more rapidly than the experimental curve. The T_1 and T_2 values predicted by our model are, in a sense, equilibrium values determined almost entirely (Fig. 2 *b*) by the free energy profile shown in Fig. 3. This is because the rates of attachment or detachment of the cross-bridge to or from actin are much slower than the time-course of the transient to T_2. Furthermore, the transition from state 1 to state 2 has not started at T_1 but is essentially complete at T_2. Therefore the specific values of α_{12} and α_{21} do not affect significantly the T_1 and T_2 curves. The other rate constants in Fig. 4 affect these

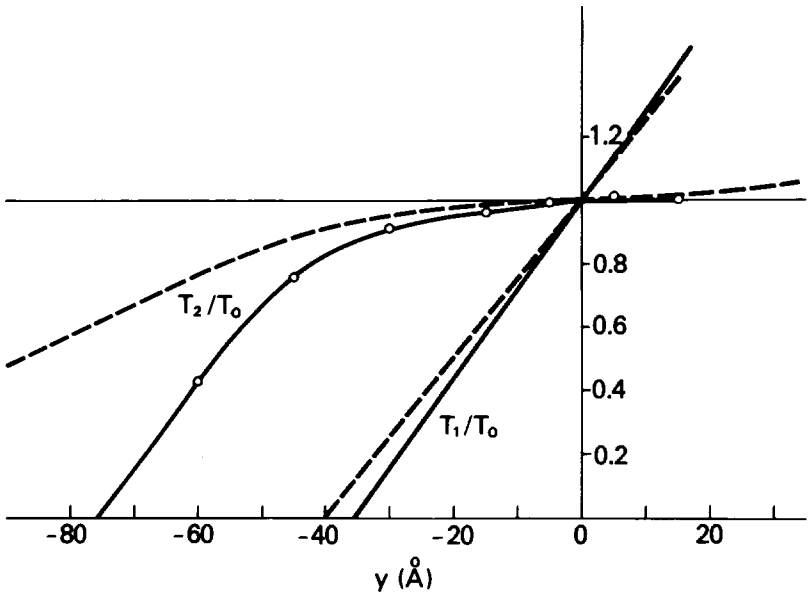

FIGURE 7 Computed and experimental values of T_1/T_0 and T_2/T_0 as functions of y (amount of release or stretch). Solid lines and open circles, computed values; dashed lines, experimental values (FHS) (4).

curves only in so far as they influence the probability of state 2 occurring at $x < 80$ Å in the isometric state.

The free energy curves in Fig. 3 for states 1 and 2 were made parabolas because the corrected experimental T_1 curve is linear (4). The 80-Å interval between free energy minima insures that $T_1 = 0$ at $y \simeq -40$ Å (actually, at $y = -35.6$ Å). The isometric distribution of cross-bridges between states 1 and 2 (Fig. 3) guarantees that the T_2 curve will have an essentially zero slope at $y = 0$. We have described in detail (Figs. 1 and 2 *b*) the approximate requirements to obtain this property. Qualitatively, although the cross-bridge distribution changes markedly between the isometric state (Fig. 5 *a*) and the time at which the T_2 level is reached (Fig. 5 *c*), the average force exerted by the cross-bridges must remain the same. This puts quite stringent requirements on the isometric distribution of states 1 and 2. It is to satisfy this requirement that we gave K_7K_{14}, the in vivo equilibrium constant between states R and 1 at $x = 80$ Å, a value of 55 (Table I). A value of 55 allows a significant number of cross-bridges to occupy state 1.

The distribution of cross-bridges in the isometric state not only explains the zero slope of the T_2 curve at $y = 0$ but also predicts that T_2 will equal zero at $y \simeq -80$ Å. In fact, experimentally, $T_2 = 0$ at approximately $y = -140$ Å. This discrepancy may arise because, in our model, after a large release, cross-bridges in state 2 detach relatively slowly and thus exert negative force at T_2. In reality the cross-bridges exerting negative force may detach more rapidly, which would have a tendency to increase the value of T_2 after large releases since fewer cross-bridges would be exerting negative force. A small amount of such detachment could occur without significantly affecting the measured stiffness.

In our model the time-courses of the force changes in isometric transients are almost

TABLE III
SCALING OF FORCE RECOVERY CURVES

y	$\frac{t_{1/2}^{-1}(\alpha)}{t_{1/2}^{-1}}$	$\frac{t_{1/10}^{-1}(\alpha)}{t_{1/10}^{-1}}$	$\frac{t_{1/2}^{-1}(\text{FHS})}{t_{1/2}^{-1}}$
Å			
−60	1.118	0.979	0.825
−45	1.134	1.001	0.987
−30	1.133	1.019	1.033
−15	1.124	1.030	0.982
− 5	1.154	1.043	0.907
+ 5	1.241	1.051	0.779
+15	1.688	1.142	0.686

completely determined by the magnitudes and x dependences of α_{12} and α_{21} (Fig. 4). These rate constants have been adjusted to fit as closely as possible the data of FHS, as already described (section 5). One of the features of the experimental data is that the rate of the return of the force to the T_2 level increases markedly as the size of the release increases. Furthermore, the time dependence of this process is not a simple exponential. However, the time dependences do seem to scale along the force and time axes. That is, although the recoveries are not exponential, if the force and time scales are adjusted linearly, all of the recoveries have the same shape. A feature of this shape is that the early part of the quick recovery of force (to T_2) is much faster than the later part.

Table III is concerned with the scaling of our theoretical isometric transients. The rate constant, α, in this table has been found from the initial slope (near $t = 0$) of a computed force recovery curve, assuming that a simple exponential recovery is followed to the T_2 level. The reciprocal time for half-recovery to T_2, following this hypothetical simple curve, would then be $t_{1/2}^{-1}(\alpha) \equiv \alpha/\ell n\, 2$. Column 2 of Table III gives the ratio of this quantity to $t_{1/2}^{-1}$ obtained from the actual computed force recovery curve. In effect, for all y except $y = +15$ Å, the initial rate constant α is ~15% larger than the half-recovery rate constant. Column 3 presents an equivalent calculation for the time: 1/10 recovery. This column shows (excluding $y = +15$ Å) that a simple exponential is essentially followed to $t_{1/10}$. Columns 2 and 3 together show that from $y = -60$ Å to $+5$ Å our computed force recovery curves have the same qualitative scaling (force and time) property that FHS observe. However, unlike FHS, the initial rate of recovery of our curves is not much faster than the later stage (to $t_{1/2}$). Because the behavior of our model is rather complicated, including x averaging, we could not find any simple explanation for the scaling phenomenon.

The last column in Table III indicates that the rate of the computed force recovery (based on $t_{1/2}^{-1}$) can be adjusted to give close to the same rate as found by FHS for steps of varying sizes. In fact, we adjusted the scale of the relevant rate constants of the model to agree in this respect with the FHS average for $y = 15, -30, -45$ Å. The calculated absolute values of $t_{1/2}^{-1}$ are plotted in Fig. 8 together with the FHS experimental curve.

8. STEADY-STATE PHYSIOLOGICAL PROPERTIES

We next examine how our model fits the steady-state physiological data obtained with frog muscle (28, 29). Fig. 9 *a* shows how the calculated force-velocity curve (solid line) compares

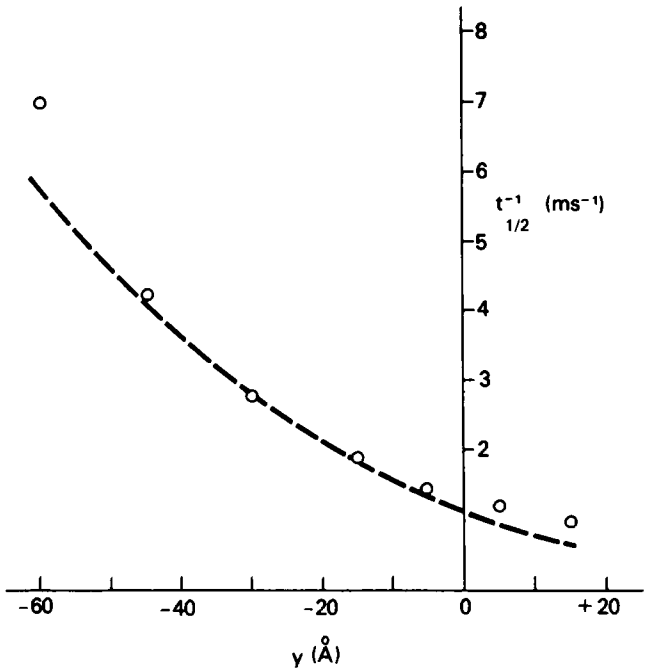

FIGURE 8 Computed and experimental values of the rate of recovery of force in the isometric transient as a function of y (amount of release or stretch). The ordinate gives $1/t_{1/2}$ as a measure of the rate constant for force recovery where $t_{1/2}$ is the time when the force has recovered one-half of the way to its T_2 value. (O) computed values; (----) experimental values (FHS) (4).

with the experimental curve (29) for frog muscle at 1.2°C (dashed line). As can be seen, the fit is quite good.

Fig. 10 presents the calculated ATPase rate and thermodynamic efficiency as a function of velocity (see Table IV for $\bar{J}_0$). Also included is $\bar{r}$, the mean number of ATP cycles per pass of an actin site past a cross bridge. As can be seen, the ATPase rate increases as the velocity increases, and is beginning to level off at high velocity at a rate approximately seven times higher than the isometric ATPase rate. Experimentally, both the rate of heat plus work production and the ATPase rate, measured directly, show a similar increase as the velocity of contraction increases (28, 35). However, the rate of heat plus work production reaches a maximum at approximately two-thirds maximal velocity and then decreases as the velocity increases still further (28, 36). Our model does not duplicate this behavior. It does, however, predict a quite reasonable efficiency. The efficiency rises rapidly as the velocity increases and then remains near 50% (37) over a broad range of velocity.

Table IV compares the calculated and experimental values of the isometric force, isometric flux, maximal efficiency, and v_m. In calculating these properties, we have assumed that there are three myosin molecules per "crown" of the myosin filament (38). As can be seen, the theoretical value for P_0 is approximately one-half the experimental value and the theoretical value of the ATPase rate in the isometric state is approximately one-third the experimental value. On the other hand, the calculated values of v_m and the maximal efficiency are in good agreement with their experimental values.

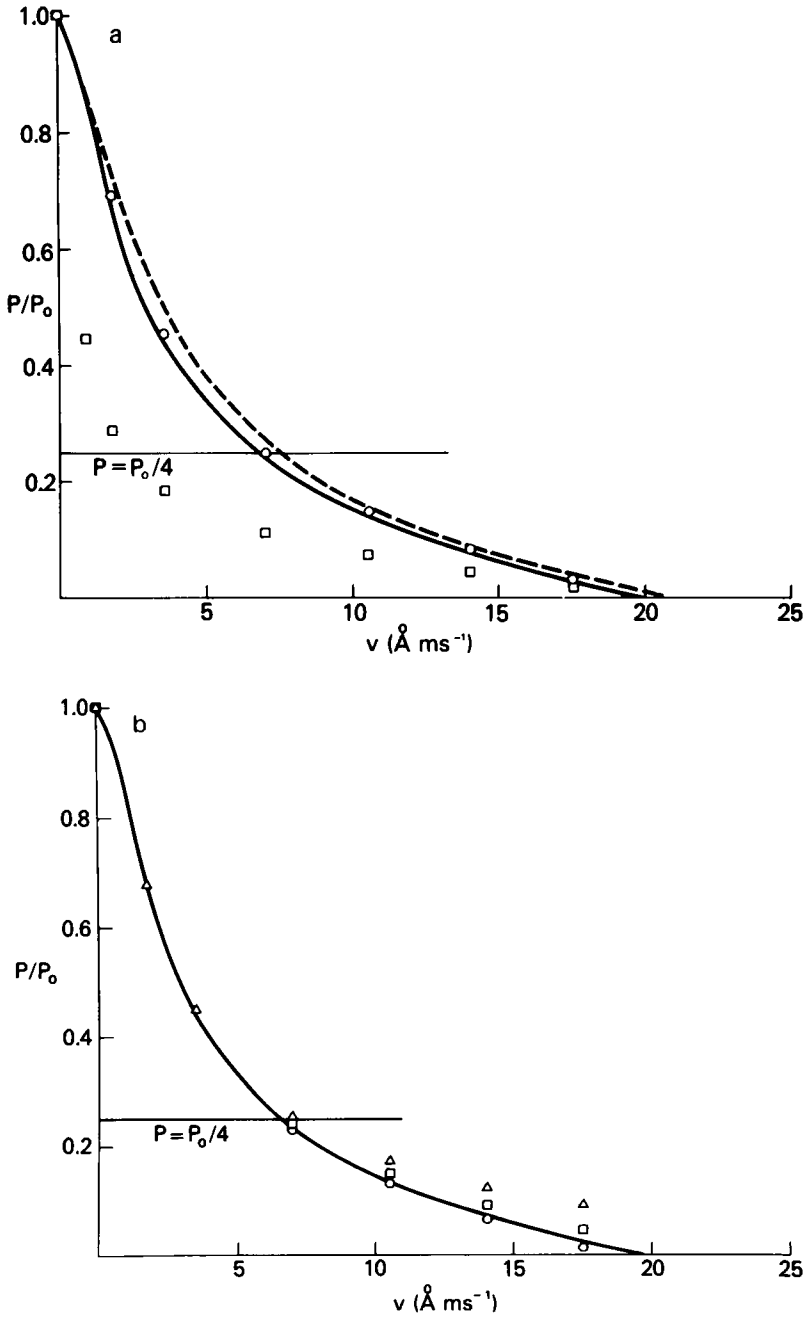

FIGURE 9 Comparison of experimental force-velocity curve with force-velocity curves calculated from our model. (*a*) (----) experimental curve for frog at 1.2°C (29); (—) curve computed from our model; (O) computed assuming a 10-fold increase in α_{N1} and α_{1N} from the values given in Fig. 4; (□) computed assuming a 10-fold reduction in the values of α_{RN} and α_{NR} (note that this assumption also leads to a reduction in the value of P_0—see text). (*b*) Change in the force-velocity curve with changes in the values assumed for α_{2R} at $x \leq -10$ Å. (—) $\alpha_{2R} = 456\ s^{-1}$, the value given in Fig. 4; (O) $\alpha_{2R} = 421\ s^{-1}$; (□) $\alpha_{2R} = 526\ s^{-1}$; (Δ) $\alpha_{2R} = 1{,}052\ s^{-1}$.

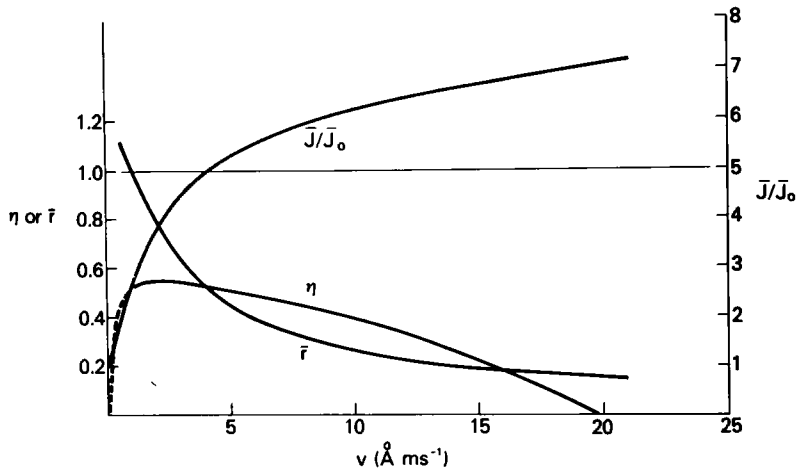

FIGURE 10 ATPase rate and efficiency calculated from the model as a function of velocity. J = ATPase rate: $\bar{J}_0$ = ATPase rate in isometric state (see Table IV for magnitude); η = efficiency (maximum = 1.0); $\bar{r}$ = mean number of ATP molecules hydrolyzed as an actin site available for attachment passes by a cross bridge.

TABLE IV
FUNDAMENTAL CONTRACTION PARAMETERS

Property	Theory	Experiment
Isometric force (P_0, T_0, F_0)	1.63×10^{-7} dyn	2.95×10^{-7} dyn (38, 39)
Isometric ATP flux (J_0)	1.15 s^{-1}	3.0 s^{-1} (40)
Isotonic v_{max}	19.8 Å ms^{-1}	21.0 Å ms^{-1} (29)
Maximal efficiency (η_{max})	0.545	0.45 to 0.66 (37)

We made no attempt to increase our calculated isometric force and ATPase rate to the actual experimental values. Clearly the isometric force and ATPase rate will depend strongly on the number of cross-bridges attached to actin in the isometric state. Since we assume in our single-site model that only approximately one-seventh of the actin monomers are available for cross-bridge attachment, most of the cross-bridges (76%) are not attached to actin in the isometric state (Table II). In our model, a cross-bridge can attach over a range of ~ 100 Å in every 360-Å period; even over this range of 100 Å, all of the cross-bridges are not attached. Thus, only about one-fourth (24%) of the cross-bridges turn out to be attached. If, as seems very likely, three or four actin monomers per turn of the actin helix are available for attachment of cross-bridges, at least twice as many cross-bridges would be attached to actin in the isometric state. This, in turn, would certainly bring both the theoretical isometric force and ATPase rate close to their experimental values. Thus, in view of the fact that we have used a single-site model (for simplicity), our values for the isometric force and ATPase rate are not unreasonable.

9. RELATIONSHIP BETWEEN ATPase RATE AND THE FORCE-VELOCITY CURVE

It is of interest to consider the key features of our model that are responsible for the steady-state properties shown in Figs. 9 *a* and 10. In particular, the force-velocity curve is

important because of the correlation (see Table VI, below) between the velocity of contraction and the actomyosin ATPase activity. This correlation between ATPase rate in vitro and velocity in vivo is the only relationship between muscle biochemistry and physiology that has thus far been documented (5).

In 1957, A. F. Huxley proposed (8) that many of the steady-state properties of muscle could be explained by having cross-bridges attach at a moderate rate (f), detach very slowly (g) in the region where they exert positive force, and detach rapidly in the region where they exert negative force. An analysis of the Huxley model shows that most of the force-velocity curve, from P_0 to approximately $P_0/4$, is practically determined by the value of f. Only when the velocity is close to v_m is the shape of the curve affected by the detachment rate in the region of negative force. The value of v_m itself depends only on this detachment rate in the Huxley model.

Why, in the Huxley model, is most of the force-velocity curve determined by the rate of attachment of the cross-bridge? A key point that any cross-bridge model must explain is the decrease in positive force exerted by the muscle as the velocity of contraction increases. This decrease in positive force can be due to a decrease in the number of attached cross-bridges that exert positive force, to an increase in the number that exert negative force, or to a combination of these effects. Which, if either, of these effects dominates in a particular model depends crucially on the rate of attachment. For example, in the Podolsky-Nolan model (27, 41), where attachment is postulated to be very rapid, there is very little decrease in the number of attached cross-bridges that exert positive force as the velocity increase. As the filaments slide past each other, cross-bridges that move out of the region where they exert positive force are replaced by others that attach rapidly. In their model the force decreases as the velocity increases because detachment of the cross-bridges that exert negative force is assumed to be quite slow. In addition, the force constant of the cross-bridge increases in the region where it exerts negative force. However, because the cross-bridges attach rapidly, the model predicts that the number of attached cross-bridges will increase as the velocity of contraction increases.

On the other hand, in the 1957 Huxley model, where attachment of the cross-bridge is postulated to be relatively slow, there is a marked decrease in the number of attached cross-bridges that exert positive force as the velocity increases. There is also a slight increase in the number that exert negative force, but this effect does not predominate until the velocity is close to v_m. Thus, in this model, the decrease in force with increasing velocity is due primarily to the relatively slow attachment rate. Consequently, this model predicts that the number of attached cross-bridges will decrease as the velocity increases. Furthermore, the slower the rate of attachment, the lower the force will be at a given velocity.

Fig. 11 shows the distribution of cross-bridges in our model as a function of velocity. We have divided the figure into two parts to avoid too many overlapping curves; the $v = 1.75$ Å ms^{-1} case provides a "bridge" between the two parts. As can be seen, our model is clearly of the Huxley type. As the velocity increases, the number of cross-bridges exerting positive force decreases markedly while the number exerting negative force increases to a much lesser extent. (State 1 has a negative force for $x < 80$ Å, state 2 for $x < 0$.) Only at very high velocity does the number exerting negative force approximately equal the greatly reduced number exerting positive force. It would therefore be expected that the total number of attached

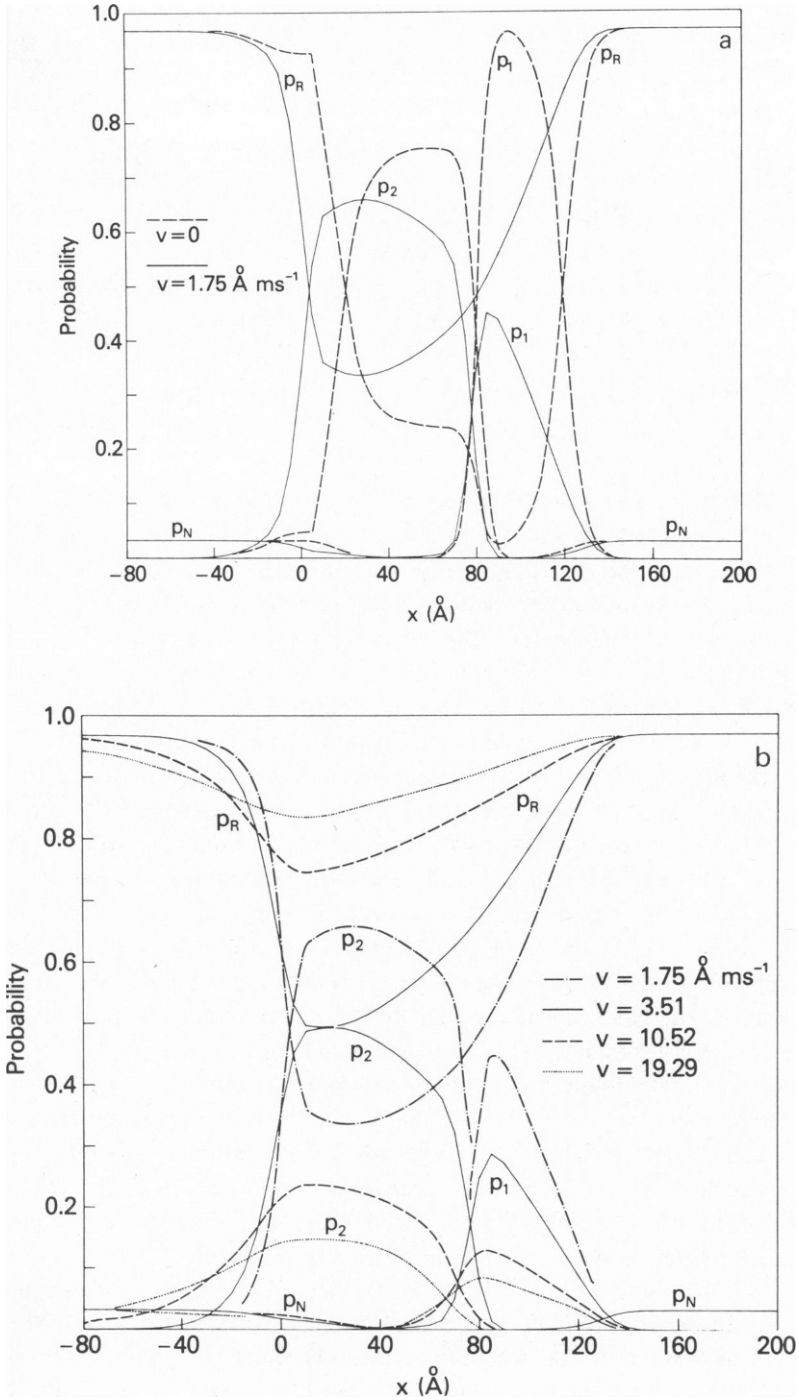

FIGURE 11 The probability distribution of cross-bridge states calculated from our model as a function of velocity. (----) isometric distribution (see also Fig. 5). Other velocities as labeled. $v = 1.75$ Å ms^{-1} is included in both *a* and *b* to facilitate comparison.

TABLE V
CALCULATED PROBABILITIES OF STATES IN ISOTONIC CONTRACTIONS

v	p_R	p_1	p_2	$\frac{(p_1 + p_2)_v}{(p_1 + p_2)_{v=0}}$
$Å\ ms^{-1}$				
0	0.736	0.1058	0.1349	1.000
1.75	0.795	0.0445	0.1391	0.763
3.51	0.843	0.0300	0.1055	0.563
10.52	0.904	0.0164	0.0581	0.310
19.29	0.925	0.0125	0.0413	0.224

cross-bridges would decrease as the velocity increases; Table V shows that this is indeed the case. The number of cross-bridges attached at v_m is 22% of the number attached in the isometric state.

If the attachment rate is closely related to the force-velocity curve, and, in turn, the force-velocity curve is correlated with the ATPase rate measured in vitro, it would be expected that the attachment rate and the ATPase rate are connected. In fact, this is exactly what is found with our model. As mentioned above, over a wide range of x the effective rate constant with which cross-bridges enter state 2, the major force-producing state is α_{RN}. Thus α_{RN} is equivalent to f in the 1957 model of A. F. Huxley. At the same time, as we discussed above, $\alpha_{RN} = k_7$, which is equal to the ATPase V_{max} per two myosin heads. Thus α_{RN} influences strongly both the force-velocity curve and the in vitro ATPase activity.

In Fig. 9 *a*, the square points show the drastic effect on the force-velocity curve of reducing α_{RN} and α_{NR} by a factor of 10. Also, the absolute value of the isometric force is reduced as a result of this change by a factor of 1.93, because fewer cross-bridges are attached in state 2.

Do any of the other rate constants alter the force-velocity curve? As long as α_{N1} is much larger than α_{RN}, it has little influence on this curve. The open circles in Fig. 9 *a* show that increasing α_{N1} and α_{1N} by a factor of 10 has almost no effect. This emphasizes that the effective attachment rate of the cross-bridge over a wide range of x is not α_{N1} but α_{RN}. The values of α_{12} and α_{21} also have almost no effect on the force velocity curve providing that, for $x < 80$ Å, α_{12} is much larger than α_{RN}, as it is in our model.

The detachment rate constant (α_{2R}) affects the force-velocity curve in two ways. In the region $x > 10$ Å, where we have assumed that α_{2r} is about one-third the effective rate of attachment α_{RN}, it is important that α_{2R} be kept significantly less than α_{RN} so that a reasonable number of cross-bridges remain in the force-producing state 2. There is, in fact, no biochemical evidence that α_{2R} is small in the region where the crossbridge exerts positive force but this would seem to be a requirement in any cross-bridge model.

The value of α_{2R} in the region $x < 0$, i.e., where the cross-bridge exerts negative force in state 2, also has an important effect on the force-velocity curve, but only on that part of the curve where P is less than $P_0/4$, i.e., where the velocity becomes quite large. As we pointed out above, the maximum velocity (v_m) is strongly influenced by α_{2R} where $x < 0$, the detachment rate in the region of negative force. In our model we make $\alpha_{2R} = 456\ s^{-1}$ where $x < -10$ Å to obtain the correct value for the maximum velocity (v_m). As already mentioned, α_{2R} represents the rate of ADP detachment from the cross-bridge. The rate constant for ADP release from

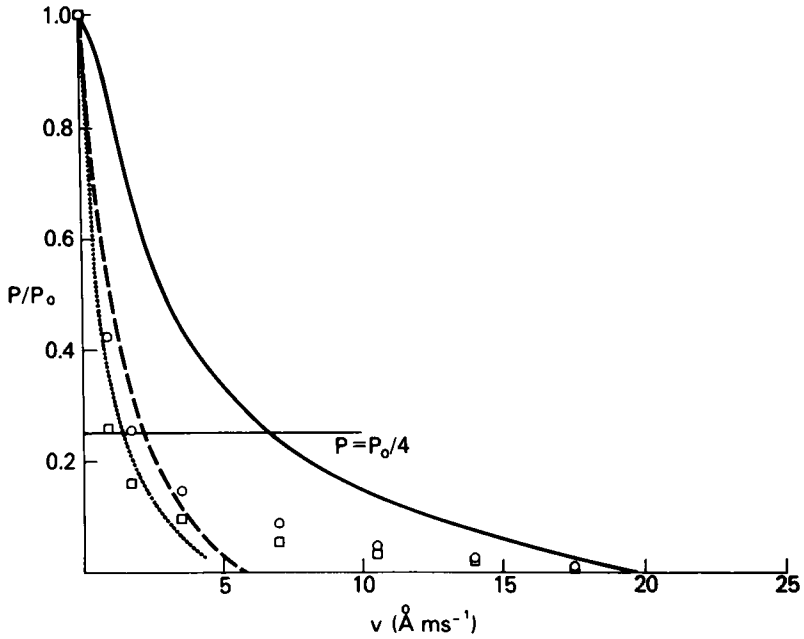

FIGURE 12 Comparison of experimental mammalian force-velocity curves with force-velocity curves computed from our model. (-----) guinea pig force-velocity curve at 10°C (42). (· · · ·) rabbit force-velocity curve at 4°C.[1] (—) Force-velocity curve computed from our model using rate constant functions given in Fig. 4. Computed assuming α_{RN}, α_{NR}, α_{2R}, and α_{R2} = 1/5 value given in Fig. 4 (O); = 1/10 value given in Fig. 4 (□).

acto-S-1 in vitro (k_{12} in Fig. 1 *a*) has not been measured with frog S-1 but it has been determined to be ~400 s^{-1} at 4°C with rabbit acto-S-1 (18).

Fig. 9 *b* shows the effect of changing α_{2R} for $x < -10$ Å (with corresponding changes in the "step" and in α_{R2}). These changes are seen to have little influence between P_0 and $P_0/4$ but, as expected, alter significantly the maximum velocity v_m. In fact, if we used $\alpha_{2R} = \infty$ for $x < -10$ Å, the force-velocity curve would change very little between P_0 and $P_0/4$ but would approach the abscissa asymptotically rather than interesecting it.

Summarizing, we find that α_{RN} is the major determinent of the force-velocity curve from P_0 to $P_0/4$, providing that the detachment rate constant, α_{2R}, in the region where state 2 exerts positive force ($x > 0$), is kept small compared to α_{RN}.

Fig. 12 shows the calculated force-velocity curves when α_{RN} and α_{2R} are both (along with α_{NR} and α_{R2}) reduced, either by a factor of 5 or a factor of 10. Because α_{2R} is changed as well as α_{RN}, the fraction of cross-bridges attached when $x < 80$ Å, in the isometric state, will remain constant despite the change in α_{RN}. For comparison, the curves for guinea pig psoas fibers at 10°C (42) and rabbit psoas fibers[1] at 4°C are also shown. Note that a reduction in α_{RN} and α_{2R} leads to curves that are quite similar, at low velocity, to the curves observed with mammalian muscle at low temperature. Qualitatively, this is what our model predicts because

[1]Tawada, K., and R. J. Podolsky. Unpublished data.

TABLE VI
RELATIONSHIP BETWEEN ATPASE ACTIVITY AND CONTRACTION VELOCITY

Conditions	Contraction velocity at $P_0/4$	Required value of α_{RN} per two myosin heads	Measured V_{max} per two HMM heads
	$Å\ ms^{-1}$	s^{-1}	s^{-1}
Frog, 1.2°C	7.5 (29)	31.8	9 (31)
Rabbit, 4°C	1.4[1]	4.3	2 (43)
Guinea pig, 6°C	1.3 (42)	4.0	2*
Guinea pig, 10°C	2.2 (42)	6.9	4*
Rabbit, 20°C	12.9‡	56.5	20 (43)

*From rabbit HMM (43) rather than guinea pig HMM.
‡From rabbit muscle at 4°C assuming $Q_{10} = 4$ (42).

experimentally the ATPase V_{max} ($=k_7 = \alpha_{RN}$) is also lower for rabbit myosin than for frog myosin.

The relationship between the contraction velocity at $P_0/4$ and the ATPase V_{max} for various muscles and temperatures is shown more quantitatively in Table VI. Column 2 shows the contraction velocity at $P_0/4$ for three kinds of muscle at several temperatures, whereas column 3 gives the values of α_{RN} (per two myosin heads) required by our model to obtain the respective contraction velocities. As can be seen, these required values of α_{RN} agree, within a factor of 2 or 3, with the measured values of V_{max} (per 2 myosin heads) shown in column 4. The results in Table VI therefore generally support our hypothesis that the rate of the transition from R to N has a strong influence on both V_{max} and the force-velocity curve from P_0 to approximately $P_0/4$. Support for our hypothesis also comes from the similar Q_{10} values reported for the mammalian force-velocity curve ($Q_{10} \simeq 4$) (29) and for V_{max} ($Q_{10} \simeq 5$) (43). Note that in Fig. 12 we made no attempt to fit the calculated v_m to the v_m observed with mammalian muscle. Obviously (see Fig. 9 *b*) we could have adjusted α_{2R} for $x < -10$ Å to give a particular v_m, but we did not do this because there is no experimental data concerning the rate of ADP release from acto-S-1 in vitro under various conditions.

10. RELATIONSHIP BETWEEN ATPASE RATE IN VITRO AND IN VIVO

Not only does α_{RN} determine both the ATPase V_{max} and the major portion of the force-velocity curve in our model, but it also establishes the ATPase rate that occurs at high velocity. In our cross-bridge model (as in any model), the overall ATP flux per cross-bridge depends on two factors: first, the fraction of cross-bridges that both attach to actin and hydrolyze ATP; and, second, the rate at which these cross-bridges hydrolyze ATP. Thus, in the isometric state, the ATP flux per cross-bridge is determined by: (*a*) the limiting rate in the ATPase cycle, which, in the isometric state, is the rate constant for cross-bridge detachment (α_{2R} for $x > 10$ Å); and (*b*) the fact that cross-bridges attach only between $x = 20$ Å and $x = 120$ Å and, furthermore, over only part of this range ($x < 80$ Å) do they hydrolyze ATP. Therefore, the ATP flux per cross-bridge in the isometric state is $\simeq \alpha_{2R}$ ($x > 10$ Å) $\times$ (60/360) $\simeq 1.5\ s^{-1}$.

During a fast isotonic contraction, the rate of cross-bridge detachment (α_{2R} for $x < -10$ Å) becomes very rapid. Therefore the rate-limiting step in the cross-bridge cycle is α_{RN}. Thus, at very high velocity, the ATP flux per cross-bridge could approach a value as high as α_{RN}.

However, even when the muscle is moving, all of the cross-bridges are not able to attach to actin all of the time. Therefore the ATP flux per cross-bridge at v_m approaches $\alpha_{RN} \times (100/360) \simeq 8\ s^{-1}$, where 100 Å is approximately the range over which the cross-bridge can attach.

If α_{RN}/α_{NR} were equal to unity rather than to 1/30, i.e., if a significant number of unattached cross-bridges occurred in state N (which attaches very rapidly to actin), the ATP flux per cross-bridge at high velocity would increase. However, it could never become larger than α_{RN}, the rate-limiting step in the ATPase cycle. Therefore, α_{RN} not only determines the force-velocity curve and V_{max}, but also strongly influences the ATP flux per cross-bridge at high velocity.

As already mentioned, we have been unable to duplicate the decrease in ATP flux per cross-bridge that occurs at high velocity according to heat measurements. A. F. Huxley has suggested (44) that the decrease in ATP flux at high velocity might be explained if the cross-bridge enters a weakly attached state before it enters the strongly attached, force-producing state. In theory, state 1 could serve as such a weakly attached state. But in our model we make α_{12} increase rapidly as x decreases so that we can obtain the very rapid rate of force recovery after large releases. As a consequence, even at very high velocity, almost all of the cross-bridges that enter state 1 transform to state 2 before they can detach from actin. Hence, although our model contains a weakly attached state, we do not obtain the observed decrease in ATP flux.

11. DISCUSSION

The most important new feature that we have presented in this paper is the incorporation of quantitative biochemical data into a specific model of muscle contraction. To employ these data, we made several basic approximations or assumptions. First, we made the approximation that, except for transitions involving attachment of the cross-bridge to actin, the equilibrium constant between any two cross-bridge states at their minimum free energies in vivo is the same as the equilibrium constant between these two states in vitro. This approximation is required if we are to make use of the in vitro biochemical data at all. It would certainly have been quite arbitrary to assume that certain equilibrium constants were the same in vivo and in vitro while others were not.

The nature of this approximation for an attached state is the following. In vivo the cross-bridge is relatively rigid when attached at the angle of minimum free energy, θ_{min}. In vitro, in the same state, new degrees of freedom are available, including fluctuations in θ around θ_{min}. These extra motions will lower the free energy of the in vitro state somewhat, relative to the in vivo state (at θ_{min}). Nevertheless, the approximation is probably accurate to within 5% in the free energy.

Even with the above approximation, one class of reactions in vivo was still not dealt with: the binding of the cross-bridge to actin. The concentration of actin in vivo has no meaning with respect to the rate of attachment of the cross-bridge. What is meant by the "effective actin concentration in vivo" is, in reality, the actin concentration required in vitro to give the same ratio $[M]:[AM]$ in vitro as occurs in vivo at $x = 0$ (cross-bridge angle = 45°). Once this single binding constant is specified (K_2 in column 3, Table I), all of the other reactions involving attachment of the cross-bridge to actin in vivo are determined by detailed balance.

For example, if in vitro the binding constant of $M^* \cdot T$ to actin is 10^7 weaker than the binding constant of M to actin, the same will be true in vivo. But to get the absolute value of the binding constant of $M^* \cdot T$ to actin in vivo, the absolute value of the binding constant of M to actin in vivo must be specified.

We and other workers have previously suggested (1, 21, 22) that the binding constants of ATP and actin to myosin should be similar, but this qualitative argument is sharpened up considerably when it is recognized that to make these binding constants alike requires an effective actin concentraion of ~10 M. By making the binding constants of ATP and actin to myosin similar, we make the free energies of the 45° state and the refractory state similar. Thus in our model there is very little loss of free energy when ATP dissociates the cross-bridge from actin; this keeps the efficiency high.

If all of the in vitro equilibrium constants were known, the approximation we made above relating in vivo and in vitro equilibrium constants, along with a value for the binding constant of the cross-bridge to actin in vivo, would determine the relative minimum free energy levels of all of the cross-bridge states in vivo. In fact, however, all of the in vitro equilibrium constants are not known. Therefore we had to make three further assumptions (Table I, column 2). One of these three assumptions is worth further mention because it has certain biochemical consequences. In our model we assumed that state $AM^* \cdot T$ does not occur to a significant extent in vivo. Often, in a cross-bridge model, a state like $AM^* \cdot T$ is assumed to be a transient intermediate without an explicit recognition of what this implies biochemically. In the present model we attempted to avoid this problem. To make state $AM^* \cdot T$ a transient intermediate, we assumed explicitly that the binding of $M^* \cdot T$ to actin is very weak. Thus we assumed that the value of K_3 in vitro is 1×10^{-1} M^{-1}. This assumption leads to two specific biochemical predictions. First, no binding should occur between $M^* \cdot T$ and actin at any actin concentration obtainable in vitro. Second, by detailed balance, $K_4 = 2 \times 10^2$ M^{-1}, that is, the binding constant of ATP to acto-S-1 in vitro should be 10^8 smaller than the binding constant of ATP to S-1.

However, very recent biochemical data (24) indicate that, at very low ionic strength, binding between $M^* \cdot T$ and actin occurs in vitro with a binding constant K_3 of $\sim 3 \times 10^4$ M^{-1}, much greater than the value assumed in our model (1×10^{-1} M^{-1}). Furthermore, by detailed balance, this result implies that $K_4 = 6 \times 10^7$ M^{-1} rather than 2×10^2 M^{-1}, as we assumed. These new biochemical data also suggest that ATP hydrolysis can occur without dissociation of the actomyosin complex and that the refractory state is able to bind weakly to actin. Clearly, if these experimental data are correct, modifications will be required in our model because the minimum free energy levels of several cross-bridge states will be changed. Possible modifications have been outlined qualitatively in a separate publication (45). Although they are of interest, they do not affect two of the major premises of the present model: first, that the transition from the 90° to the 45° state is mainly responsible for the recovery of force in the isometric transient; and, second, that the transition from the refractory to the nonrefractory state has a major influence on both the force-velocity curve and the ATPase rate. Nevertheless, the very fact that our model is sensitive to changes in the minimum free energy levels of the cross-bridge states emphasizes the importance of biochemical data in determining the properties of a cross-bridge model.

Not only the free energy levels but also the rate constants in our model are dependent on the

in vitro biochemical data. One example is our assumption that the transition from the 90° to the 45° state is very fast in vivo; this is related to kinetic evidence suggesting that the transition from $AM\dagger \cdot D \cdot P_i$ to $AM^* \cdot D$ is quite rapid in vitro (6). An even better example is our assumption that the transition from the refractory to the nonrefractory state has the same rate in vivo and in vitro. This is the feature of our model that is the most successful in relating biochemistry and physiology: it provides a possible explanation for the well-known relationship between ATPase activity in vitro and the velocity of muscle contraction in vivo. It is interesting that data obtained with cardiac muscle from normal and thyrotoxic animals also showed a correlation between the velocity of contraction and the ATPase V_{max} (46). As accurate force-velocity curves and values of V_{max} are obtained for more types of muscle, the quantitative relationship between ATPase rate and velocity predicted by our model will be repeatedly tested.

Although our model provides a possible explanation for the relationship between ATPase rate and the velocity of contraction v, as in any model where the force-velocity curve is essentially established by the effective rate of attachment, ours predicts that the number of attached cross-bridges decreases markedly as v increases. Actually, one interpretation (47) of x-ray measurements on contracting frog muscle is that there is little if any change in the number of attached cross-bridges as v increases. If one accepts this interpretation, it is possible that recent biochemical data, which indicates that not only the nonrefractory state but also the refractory state binds weakly to actin, could explain the x-ray results. If the refractory state is weakly attached to actin, the number of attached cross-bridges might not decrease as v increases. Nevertheless, the transition from the refractory to the nonrefractory state could still limit the rate at which the major force-producing 45° state is formed and hence determine the velocity of contraction (45). We are planning further modeling efforts to investigate whether this modified refractory state model can explain the correlation between ATPase rate and velocity of contraction without predicting a marked decrease in the number of attached cross-bridges as v increases.

Received for publication 15 May 1979 and in revised form 31 August 1979.

REFERENCES

1. EISENBERG, E., and T. L. HILL. 1978. A cross-bridge model of muscle contraction. *Prog. Biophys. Mol. Biol.* **33**:55.
2. HILL, T. L. 1974. Theoretical formalism for the sliding filament model of contraction of striated muscle. Part I. *Prog. Biophys. Mol. Biol.* **28**:267.
3. HILL, T. L. 1977. *Free Energy Transduction in Biology.* Academic Press, New York.
4. FORD, L. E., A. F. HUXLEY, and R. M. SIMMONS. 1977. Tension responses to sudden length change in stimulated frog muscle fibres near slack length. *J. Physiol. (Lond.).* **269**:441.
5. BARANY, M. 1967. ATPase activity of myosin correlated with speed of muscle shortening. *In* The Contractile Process. Little, Brown and Co., Boston. 197.
6. CHOCK, S. P., P. B. CHOCK, and E. EISENBERG. 1976. Pre-steady-state kinetic evidence for a cyclic interaction of myosin subfragment one with actin during the hydrolysis of ATP. *Biochemistry.* **15**:3244.
7. HUXLEY, A. F., and R. M. SIMMONS. 1971. Proposed mechanism of force generation in striated muscle. *Nature (Lond.)* **233**:533.
8. HUXLEY, A. F. 1957. Muscle structure and theories of contraction. *Prog. Biophys. Biophys. Chem.* **7**:255.
9. GOODY, R. S., W. HOFMANN, and H. MANNHERZ. 1977. The binding constant of ATP to myosin S1 fragment. *Eur. J. Biochem.* **78**:317.

10. WOLCOTT, R. G., and P. D. BOYER. 1974. The reversal of the myosin and actomyosin ATPase reactions and the free energy of ATP binding to myosin. *Biochem. Biophys. Res. Commun.* **57**:709.
11. MARSTON, S., and A. WEBER. 1975. The dissociation constant of the actin-heavy meromyosin subfragment-1 complex. *Biochemistry.* **14**:3868.
12. GREENE, L. E., and E. EIESENBERG. 1978. Formation of a ternary complex: actin, 5'-adenylyl imidodiphosphate, and the subfragments of myosin. *Proc. Natl. Acad. Sci. U.S.A.* **75**:54.
13. BAGSHAW, C. R., and D. R. TRENTHAM. 1973. The reversibility of ATP cleavage by myosin. *Biochem. J.* **133**:323.
14. TAYLOR, E. W. 1977. Transient phase of ATP hydrolysis by myosin, heavy meromyosin, and subfragment 1. *Biochemistry.* **16**:732.
15. CHOCK, S., and E. EISENBERG. 1978. The mechanism of the skeletal muscle myosin ATPase. I. Identity of the myosin active sites. *J. Biol. Chem.* **254**:3229.
16. LOWEY, S., and S. M. LUCK. 1969. Equilibrium binding of ADP to myosin. *:Biochemistry.* **8**:3195.
17. GREENE, L. E., and E. EISENBERG. Dissociation of the actin subfragment-one complex by 5'-adenylyl imidodiphosphate, ADP, and PP_i. *J. Biol. Chem.* In press.
18. WHITE, H. D. 1977. Magnesium-ADP binding to acto-myosin-S1 and acto-heavymeromyosin. *Biophys. J.* **17**:40*a*.
19. ALBERTY, R. A. 1968. Effect of pH and metal ion concentrations on the equilibrium hydrolysis of ATP to ADP. *J. Biol. Chem.* **243**:1337.
20. DAWSON, M. J., P. G. GADIAN, and D. R. WILKIE. 1978. Muscular fatigue investigated by phosphorus nuclear magnetic resonance. *Nature (Lond.).* **274**:861.
21. MORALES, M. F. 1975. A guide to the muscle papers. *J. Supramol. Struct.* **3**:105.
22. HIGHSMITH, S., R. A. MENDELSON, and M. F. MORALES. 1976. Affinity of myosin S-1 for F-actin, measured by time-resolved fluorescence anisotropy. *Proc. Natl. Acad. Sci. U.S.A.* **73**:133.
23. WHITE, H. D., and E. W. TAYLOR. 1976. Energetics and mechanism of actomyosin ATPase. *Biochemistry.* **15**:5818.
24. STEIN, L. A., R. SCHWARZ, P. B. CHOCK, and E. EISENBERG. The mechanism of the actomyosin ATPase: evidence that ATP hydrolysis can occur without dissociation of the actomyosin complex. *Biochemistry.* **38**:3895.
25. HILL, T. L. 1975. Theoretical formalism for the sliding filament model of contraction of striated muscle. Part II. *Prog. Biophys. Mol. Biol.* **29**:105.
26. HILL, T. L., and E. EISENBERG. 1979. Simplified theory of the Huxley-Simmons T_0, T_1 and T_2 in muscle models with two attached states. *In* The Role of Cross-Bridges in Muscle Contraction. H. Sugi and G. H. Pollack, editors. University of Tokyo Press, Tokyo. 541.
27. HILL, T. L., E. EISENBERG, Y. CHEN, and R. J. PODOLSKY. 1975. Some self-consistent two-state sliding filament models of muscle contraction. *Biophys. J.* **15**:335.
28. HUXLEY, A. F. 1974. Muscular contraction. *J. Physiol. (Lond.).* **243**:1.
29. EDMAN, K. A. P., and J. C. HWANG. 1977. The force-velocity relationship in vertebrate muscle fibres at varied tonicity of the extracellular medium. *J. Physiol. (Lond.).* **269**:255.
30. EISENBERG, E., and C. MOOS. 1968. The ATPase activity of acto-heavy meromyosin. A kinetic analysis of actin activation. *Biochemistry.* **7**:1486.
31. FERENCZI, M., E. HOMSHER, D. R. TRENTHAM, and A. G. WEEDS. 1978. Preparation and characterization of frog muscle myosin subfragment-1 and actin. *Biochem. J.* **171**:155.
32. EISENBERG, E., and W. W. KIELLEY. 1972. Evidence for a refractory state of HMM and S-1 unable to bind to actin in the presence of ATP. *Cold Spring Harbor Symp. Quant. Biol.* **37**:145.
33. RIZZINO, A. A., W. W. BAROUCH, E. EISENBERG, and C. MOOS. 1970. Actin-heavy meromyosin binding. Determination of binding stoichiometry from ATPase kinetic measurements. *Biochemistry.* **9**:2402.
34. FORD, L. E., A. F. HUXLEY, and R. M. SIMMONS. 1974. Mechanism of early tension recovery after a quick release in tetanized muscle fibers. *J. Physiol. (Lond.).* **240**:42.
35 KUSHMERICK, M. J., and R. E. DAVIES. 1969. The chemical energetics of muscle contraction. II. The chemistry, efficiency and power of maximally working sartorius muscles. *Proc. R. Soc. B* **174**:315.
36. HILL, A. V. 1964. The effect of load on the heat of shortening of muscle. *Proc. R. Soc. B.* **159**:297.
37. WILKIE, D. R. 1975. Muscle as a thermodynamic machine. *In* Energy Transformation in Biological Systems. Ciba Foundation Symposium 31 (new series). Elsevier, Amsterdam. 327.
38. TREGEAR, R. T., J. M. SQUIRE, 1973. Myosin content and filament structure in smooth and striated muscle. *J. Mol. Biol.* **77**, 279.
39. GORDON, A. M., A. F. HUXLEY, and F. J. JULIAN. 1966. The variation in isometric tension with sarcomere length in vertebrate muscle fibers. *J. Physiol. (Lond.).* **184**:170.

40. CURTIN, N. A., C. GILBERT, K. M. KRETZSCHMAR, and D. R. WILKIE. 1974. The effect of the performance of work on total energy output and metabolism during muscular contraction. *J. Physiol. (Lond.)*. **238**:455.
41. PODOLSKY, R. J., and C. NOLAN. 1973. Muscle contraction transients, cross-bridge kinetics, and the Fenn effect. *Cold Spring Harb. Symp. Quant. Biol.* **37**:661.
42. GULATI, J. 1976. Force-velocity characteristics for calcium-activated mammalian slow-twitch and fast-twitch skeletal fibers from the guinea pig. *Proc. Natl. Acad. Sci. U.S.A.* **73**:12.
43. BAROUCH, W., and C. MOOS. 1971. Effect of temperature on actin activation of heavy meromyosin ATPase. *Biochim. Biophys. Acta.* **234**:183.
44. HUXLEY, A. F. 1973. A note suggesting that the cross-bridge attachment during muscle contraction may take place in two stages. *Proc. R. Soc. B.* **183**:83.
45. EISENBERG, E., and L. E. GREENE. 1980. The relation of muscle biochemistry to muscle physiology. *Annu. Rev. Physiol.* In press.
46. BANERJEE, S. K., E. G. KABBAS, and E. MORKIN. 1977. Enzymatic properties of the heavy meromyosin subfragment of cardiac myosin from normal and thyrotoxic rabbits. *J. Biol. Chem.* **252**:6925.
47. PODOLSKY, R. J., R. ST. ONGE, L. YU, and R. W. LYMN. 1976. X-ray diffraction of actively shortening muscle. *Proc. Natl. Acad, Sci. U.S.A.* **64**:504.